

UNCLASSIFIED

AD 295 144

*Reproduced
by the*

**ARMED SERVICES TECHNICAL INFORMATION AGENCY
ARLINGTON HALL STATION
ARLINGTON 12, VIRGINIA**



UNCLASSIFIED

NOTICE: When government or other drawings, specifications or other data are used for any purpose other than in connection with a definitely related government procurement operation, the U. S. Government thereby incurs no responsibility, nor any obligation whatsoever; and the fact that the Government may have formulated, furnished, or in any way supplied the said drawings, specifications, or other data is not to be regarded by implication or otherwise as in any manner licensing the holder or any other person or corporation, or conveying any rights or permission to manufacture, use or sell any patented invention that may in any way be related thereto.

63-2-3

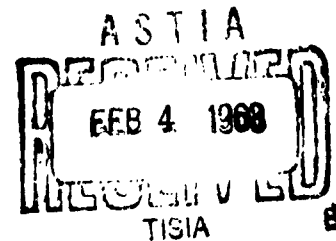
MEMORANDUM
RM-3270-PR
JANUARY 1963

295 144

CATALOGED BY ASTIA
AS AD No. _____

THE GROWTH OF
THE HYPERSONIC TURBULENT WAKE
BEHIND BLUNT AND SLENDER BODIES

Paul S. Lykoudis



PREPARED FOR:
UNITED STATES AIR FORCE PROJECT RAND

The **RAND** Corporation
SANTA MONICA • CALIFORNIA

MEMORANDUM

RM-3270-PR

JANUARY 1963

**THE GROWTH OF
THE HYPERSONIC TURBULENT WAKE
BEHIND BLUNT AND SLENDER BODIES**

Paul S. Lykoudis

This research is sponsored by the United States Air Force under Project RAND - Contract No. AF 49(638)-700 - monitored by the Directorate of Development Planning, Deputy Chief of Staff, Research and Technology, Hq USAF. Views or conclusions contained in this Memorandum should not be interpreted as representing the official opinion or policy of the United States Air Force. Permission to quote from or reproduce portions of this Memorandum must be obtained from The RAND Corporation.

The **RAND** *Corporation*

1700 MAIN ST • SANTA MONICA • CALIFORNIA

PREFACE

This Memorandum is a part of continuing RAND studies on the behavior of bodies re-entering the atmosphere at high velocities. The results should be of interest to those engaged in predicting, understanding, and evaluating the characteristics of hypersonic trails in the atmosphere.

SUMMARY

An attempt is made to develop a theory for the calculation of the growth of the turbulent wake formed behind a blunt body moving at hypersonic speeds. The classical, semiempirical subsonic-wake theory based on the notion of eddy diffusivity is used throughout, duly modified to account for compressibility effects. The gas is assumed to be in thermodynamic equilibrium. A number of suitable approximations are made, resulting in a closed-form solution.

Several plots showing the growth of the width of the turbulent core downstream are presented for different Mach numbers and different values of the enthalpy prevailing at the center of the "neck" of the wake. It is found that compressibility effects for blunt bodies are limited in general up to about 1000 diameters downstream. Beyond this distance the wake grows with the $1/3$ power rule, like a subsonic incompressible wake, with no dependence on the Mach number.

The fundamental equations are also written for sharp bodies for which the boundary-layer effects are important. It is found that the enthalpy decay along the axis downstream is faster for thin bodies than it is for blunted ones.

ACKNOWLEDGMENTS

The author wishes to express his sincere appreciation to Dr. Leslie Hromas of Space Technology Laboratories for communicating new results from his work and for many stimulating discussions. He also acknowledges with thanks the many useful comments, discussions, and suggestions he received from his colleagues at RAND--Mary Romig, Carl Gazley, Jr., Joseph Gross, and C. Forbes Dewey, Jr.--and the numerical computations performed by Jeannine McGann.

CONTENTS

PREFACE	iii
SUMMARY	v
ACKNOWLEDGMENTS	vii
SYMBOLS	xi
Section	
I. INTRODUCTION	1
II. ANALYSIS AND RESULTS FOR THE CASE OF BLUNT BODIES	10
III. ANALYSIS FOR THE CASE OF CONES AND SLENDER BODIES	23
IV. CONCLUSIONS	35
Appendix	
A. CALCULATION OF THE VELOCITY PREVAILING AT THE POINT ON THE AXIS WHERE THE PRESSURE IS ALMOST AMBIENT IN THE INVISCID WAKE OF A BLUNT BODY	37
B. INFLUENCE OF THE LAMINAR COOLING AT THE FRONT OF THE TURBULENT WAKE	39
C. EVALUATION OF THE FUNCTIONS A AND C_{Df} IN TERMS OF THE HOWARD VARIABLE R	41
D. CALCULATION OF \bar{r} IN TERMS OF THE HOWARD VARIABLE R FOR BLUNT BODIES	44
E. STUDY OF THE FUNCTION $\bar{r}_f(\bar{x})$ FOR DIFFERENT MACH NUMBERS AND DIFFERENT ENTHALPIES PREVAILING AT THE CENTER OF THE NECK OF A BLUNT BODY	45
F. APPROXIMATION OF EQ. (39) WITH EQ. (44)	52
REFERENCES	55

SYMBOLS

- A = excess amplitude of turbulent-enthalpy profile, defined in Eq. (19)
 a = numerical constant used in Eqs. (2) and (10)
 B = parabolic "width" of turbulent-enthalpy profile, defined in Eq. (20)
 C_D = drag coefficient
 d = body diameter
 f = velocity ratio defined in Eq. (5)
 H = nondimensional enthalpy, defined in Eq. (7)
 h = enthalpy
 \bar{h}_f = h_f/h_∞
 M = free-stream Mach number
 p = pressure
 R = Howarth variable in the radial direction, defined in Eq. (4)
 R_s = nondimensional co-ordinate describing bow shock wave
 R_T = turbulent variable in the radial direction, defined in Eq. (14)
 r = radial co-ordinate
 r_o = nose radius
 \bar{r} = r/r_o
 U_∞ = free-stream velocity
 u = velocity in the x direction
 x = co-ordinate along the direction of the free stream
 x_o = distance downstream at which the pressure is ambient for every streamline, given by Eq. (1)
 \bar{x} = x/d
 γ = ratio of specific heats, c_p/c_v

- γ_L = numerical constant used in Eq. (2)
- \mathcal{E} = compressible eddy diffusivity defined in Eq. (12)
- ϵ = eddy diffusivity defined in Eq. (15)
- κ = numerical coefficient used for the definition of the eddy diffusivity
- λ = fraction of the stagnation enthalpy calculated at the "neck" of the turbulent core; see Eq. (35)
- ρ = mass density

SUBSCRIPTS

- f = the turbulent front
- i = an initial condition
- ∞ = the free stream

I. INTRODUCTION

It is a matter of common observation that the motion of bodies in fluids produces a trail which very often persists over distances many times the characteristic length of the body. Theoretical and experimental studies consist primarily of descriptions of the distribution of momentum defect downstream. At low speeds this defect is associated with the viscous layer only. At supersonic speeds, however, the major part of the momentum defect for a blunt object is due to the irreversibility created by the shock wave. The maximum irreversibility (and hence the maximum defect) for an axisymmetric body appears on the axis parallel to the flow where the shock is normal, with smaller irreversibilities and hence smaller momentum defects, corresponding to streamlines located farther away from the axis.

The structure of the flow for a spherical object moving at hypersonic speeds can be seen in Fig. 1. The fluid is compressed through the bow shock wave and expanded isentropically until it is recompressed again by the so-called trailing shock. Then it expands again until all streamlines reach the ambient pressure at a distance denoted by $x = x_0$. This distance can be calculated as indicated in Ref. 1 by using the blast-wave theory, although this theory allows only for the bow shock wave and neglects the details of the flow from the bow shock to the point $x = x_0$. The latter has been shown in Refs. 1 and 2* to create a small amount of irreversibility when compared with the bow shock wave, so that if one is interested in calculating the flow at a distance far enough downstream, its influence can be neglected in a first approximation. In nondimensional terms, the distance x_0 is given in Ref. 1 as

$$\frac{x_0}{d} \approx \frac{M^2}{9} \quad (1)$$

In the above, d is the diameter of the sphere and M is the free-stream

*Also private communication from L. Hromas, Space Technology Laboratories.

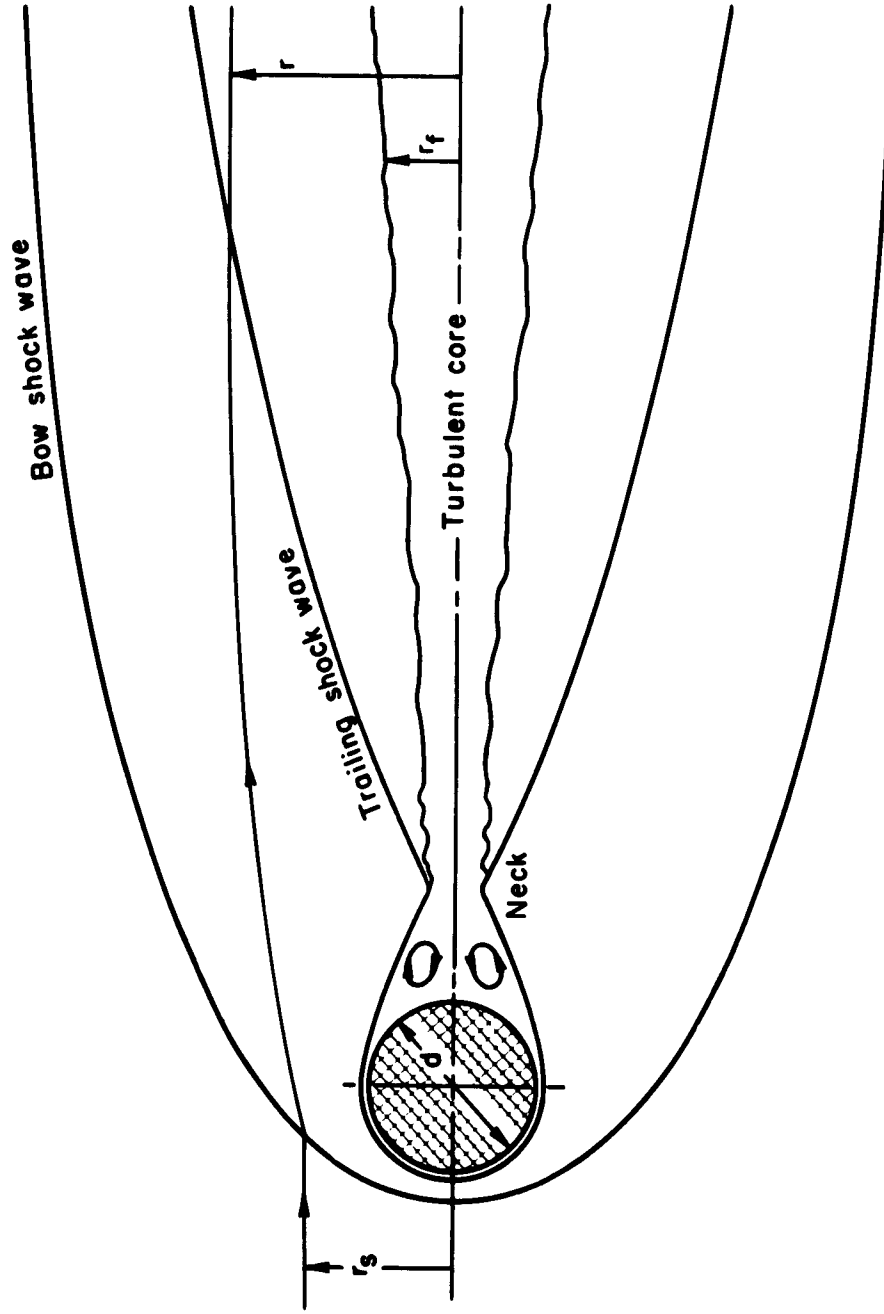


Fig. 1— Nomenclature for the wake behind a sphere
at hypersonic speeds

Mach number. Feldman, in Ref. 2, was the first to analyze the flow of a hypersonic trail around a blunt body. By standard numerical techniques he calculated the flow around a hemisphere followed by a cylinder by assuming inviscid flow of a real gas in thermodynamic equilibrium. At the cross section $x = x_0$ he assumed that the enthalpy profile is given by a Gaussian distribution, the width of which he obtained by a best fit of his numerical results. From there on he assumed that further cooling occurred by the mechanism of heat conduction only. He was thus able to determine all thermodynamic parameters, including electron concentration, up to the point where the ambient state is reached.

In Ref. 1 it was shown that the inviscid enthalpy profile at the cross section $x = x_0$ can be approximated analytically in a closed form by assuming a parabolic bow shock wave as given by the cylindrical-blast-wave theory. The result is

$$\frac{h_{x_0}(R)}{h_{x_0}(0)} = \frac{1}{\left(1 + \frac{4R_s}{aC_D}\right)^{1/\gamma_L}} \quad (2)$$

In the above, R_s is the nondimensional radius (with respect to the radius of the nose r_0) determining a stream tube entering the bow shock wave (see Fig. 1) and is related to the nondimensional radius $\bar{r} = r/r_0$ of the same stream tube at the cross section $x = x_0$ by the equation of mass continuity

$$\rho_\infty U_\infty R_s dR_s = \rho_{x_0} u_{x_0} \bar{r} d\bar{r} \quad (3)$$

Feldman indicated from his numerical calculations that the ratio $u_{x_0}/U_\infty \approx 0.8$, so in this sense the radius R_s is almost equivalent to the Howarth variable R , given as

$$fR^2 \approx R_s^2 \quad (4)$$

where

$$f = u_{x_0}/U_\infty \quad (5)$$

In Appendix A it is shown that f is given approximately in a closed form by the expression

$$f = \sqrt{1 - \frac{1}{3\sqrt{M}}} \quad (6)$$

For Mach numbers between 15 and 35, f varies between 0.77 and 0.83, and it is thus seen that the Mach-number dependence is indeed very weak. From the condition that the stagnation enthalpy remains constant everywhere in the inviscid flow field, we obtain

$$H = \frac{h_{x_0}(0)}{h_\infty} = 1 + \frac{(1 - f^2)(\gamma - 1)M^2}{2} \quad (7)$$

For the quantity f , Eq. (6) could be substituted above, thus obtaining Eq. (A-2) again; however, if we enter the value $f = 0.8$, the result is a good approximation for Mach numbers of 10 and above to the exact values that can be obtained by using real-gas effects. Also, by neglecting unity compared to the term containing the Mach number in Eq. (7), we obtain

$$H = \frac{(\gamma - 1)M^2}{6} \quad (8)$$

The parameter a in Eq. (2) and the drag coefficient C_D^* determine the shape of the shock wave from blast-wave theory to be

$$R_s = (aC_D^*)^{1/4} \sqrt{\frac{x}{r_0}} \quad (9)$$

*This coefficient accounts only for the pressure drag.

The parameter γ_L is an effective c_p/c_v ratio, which as shown in Ref. 1 has the approximate value of 1.2. The value of a is approximately equal to 2.6.

In Ref. 1 it was also shown that a good approximation of Eq. (2) is

$$\frac{h_{x_0}(R)}{h_\infty} \approx \frac{H}{1 + \frac{4f^2 R^2}{a\gamma_L C_D}} \approx \frac{H}{1 + \frac{R^2}{C_D}} \quad (10)$$

In the above, the values of $f \approx 0.8$, $a = 2.6$, and $\gamma_L = 1.2$ have been used. This relation is in good agreement with numerical results obtained through the method of characteristics in Refs. 2 and 3. A comparison is shown in Fig. 2, where the exact value for H was used in Eq. (10) rather than the approximation of Eq. (8).

Further inspection of Fig. 1 shows that the trailing shock is formed around a "neck" which presumably contains the mass flowing through the boundary layer over the sphere. From the point of view of total momentum defect (and hence drag) contained in the neck, simple calculations by Lees and Hromas show that for a typical hypersonic flight this amount is very small compared with the total drag.⁽³⁾ They point out that this drag represents the sum of the skin-friction drag on the body and the momentum defect associated with the pressure rise across the trailing shock at the neck. Their estimate of these two contributions at the neck is given for the cylindrical case as

$$(C_D)_{\text{neck}} \approx \frac{5}{\sqrt{Re}} \quad (11)$$

This result should be multiplied by $\sqrt{2}$ for the axisymmetric case. The Reynolds number is based on the diameter and free-stream conditions.

Turbulence is always associated with regions of high vorticity, which in the present case is the free shear layer formed after

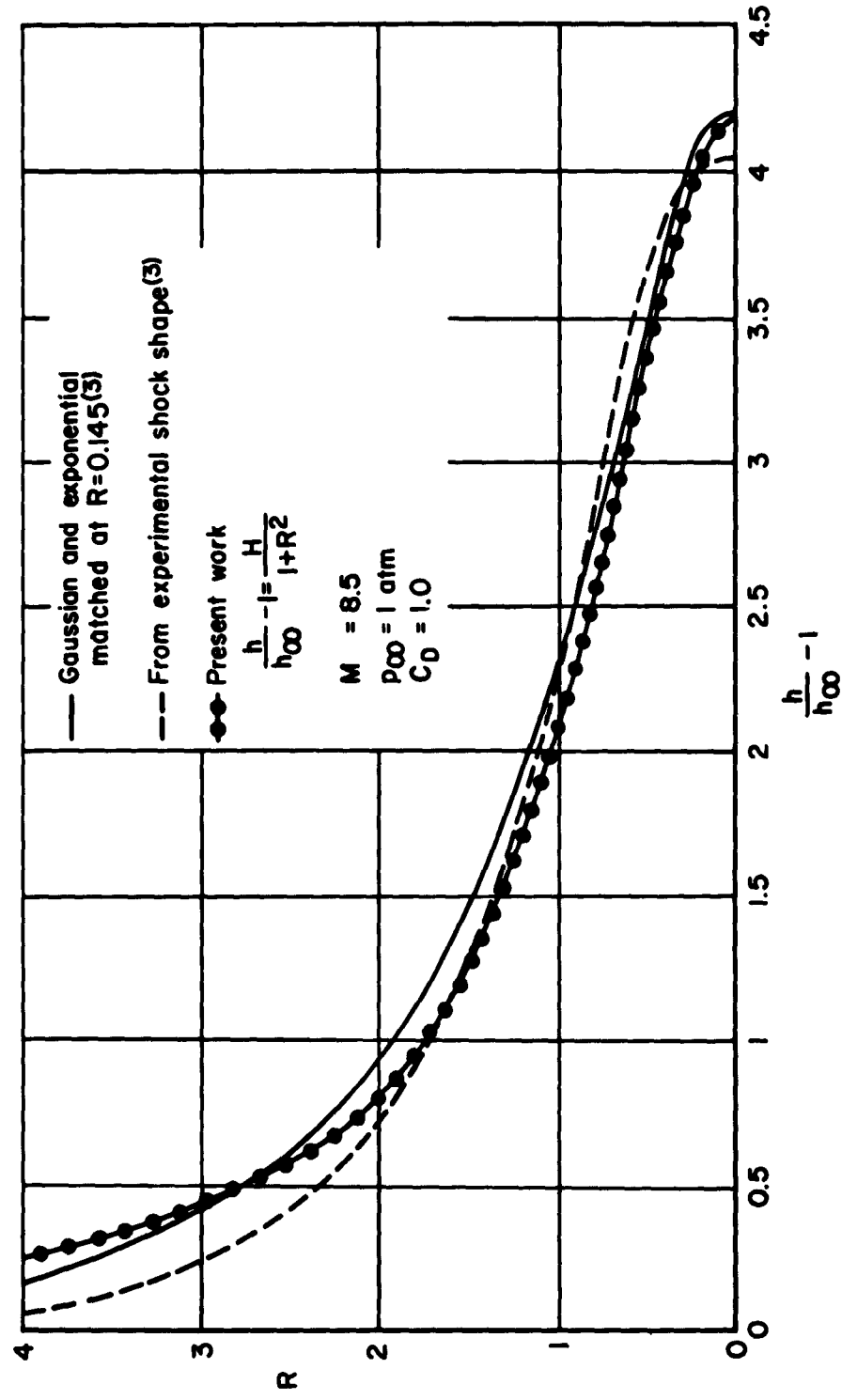


Fig. 2 — Inviscid enthalpy profiles from Ref 3 compared with present work for $M = 8.5$

separation occurs. Although conclusive experimental study of the so-called "near wake" region is still lacking,* we shall assume that turbulence is present in the region near the neck, engulfing the fluid mass downstream that has gone over the blunt body through the inviscid part of the wake. The "engulfing" mechanism for the first few diameters downstream of the neck will be dictated solely by expansion, since just behind the trailing shock the temperature and pressure are very high. As the pressure drops to nearly ambient, turbulent diffusion will become predominant--swallowing up more and more momentum and finally spreading to a point where the whole momentum deficiency is associated with turbulence.

A calculation based on the above model needs the following a priori knowledge: (a) the position and thickness (in terms of mass, momentum, and energy) of the neck, (b) pressure profiles downstream of the neck, and (c) a model for the estimation of the rate of energy diffusion due to turbulence. The first two items presume the solution of the near-wake problem with an answer describing the interaction of the trailing shock with the free shear layer, a rather difficult and still unsolved problem. As a rough approximation one may obtain some information for the first two items by solving the inviscid problem over a sphere followed by a cone, which takes the place of the shear layer, and then a cylinder fitted at the neck. Shadowgraph pictures can be used for guidance in prescribing the above geometry. Such calculations are reported in Ref. 3. For item (c) the only choice offered is the extension of the subsonic eddy-diffusivity theories to the compressible case. Such an extension is provided in Refs. 3 and 5. Both references present an equivalent eddy diffusivity \mathcal{E} given in terms of the incompressible eddy diffusivity ϵ as

$$\mathcal{E} = \left[\frac{\rho(0)}{\rho_f} \right]^{\frac{2}{1+j}} \epsilon \quad (12)$$

*Some preliminary results are reported in Ref. 4.

In the above, $\rho(0)$ indicates the mass density at the axis, and ρ_f the density at the "front" of the turbulent core (see Fig. 1); j takes the value 0 for the two-dimensional case and 1 for the axisymmetric.

At this point let it be stated that there is no rigorous theoretical understanding even of the rudiments of shear turbulence; what has been accomplished over so many years of study is the replacement of our ignorance by one or more "factors of adjustment" which can be conveniently selected to fit the experiments. For instance, for turbulent flow in a pipe we have the numerical coefficient of proportionality yielding the linear law of variation of the mixing length, whereas for wakes we select the numerical value of a constant of proportionality yielding ϵ , a number akin to a Reynolds number. Now ϵ (as will be seen later) is also proportional to the drag coefficient, and in the problem at hand, the drag associated with the turbulent core is variable in the direction of the stream.* It is therefore suggested in Ref. 3 that experimental evidence should also be used in deciding between the two extreme cases of a coefficient proportional to a frozen drag (say the one at the neck) or local drag.

From a logical point of view one necessarily concludes that the artificial mechanisms of eddy diffusivity and mixing length explain nothing of the true nature of turbulence. In essence they are used to provide definitions and numerical values for quantities whose intrinsic existence can be justified only by the fact that they sometimes provide adequate answers in much wider regions of observation without additional forcing, although they are adjusted to satisfy the experimental evidence in a restricted area. From this point of view, the merit of a semiempirical theory is judged by the degree of universality of the answer for a minimum number of factors of adjustment.

Bearing this in mind, we will attack the problem at hand by assuming that the inviscid-enthalpy profile prevailing in the "laminar region" is given by Eq. (10). Inside the turbulent core we assume a parabolic profile extending up to the distance \bar{r}_f characterizing the turbulent front.

*In contrast to the subsonic case in which the turbulent core encompasses all the drag.

In the limit $r \rightarrow 0$, where the energy equation will be satisfied in detail along the axis, a parabolic profile is the only one satisfying this equation. In the radial direction, energy will be conserved in bulk between $r = 0$ and $r = \infty$ in the fashion of the well-known boundary-layer integral methods. We will compute eddy diffusivity through Eq. (12), using for ϵ its incompressible definition,⁽⁶⁾ and bearing in mind that this definition is strictly valid only in the neighborhood of the axis of symmetry.

In every physical detail the above is the physical model adopted by Lees and Hromas;⁽³⁾ however, the mathematical model and approximations of the present work are different, yielding a closed-form solution rather than a solution necessitating extensive numerical calculations.

II. ANALYSIS AND RESULTS FOR THE CASE OF BLUNT BODIES

The equation of conservation of energy for an axisymmetric wake is

$$\rho u \frac{\partial h}{\partial x} = \frac{1}{r} \frac{\partial}{\partial r} \left(\rho \epsilon r \frac{\partial h}{\partial r} \right) \quad (13)$$

Here again ϵ is the Boussinesq turbulent eddy diffusivity. For the velocity u , we set

$$u = f U_{\infty}$$

where f is between 0.8 and 1.0.

In Eq. (13) we have neglected the contribution of the normal velocity component in the convective heat transfer, any cooling due to pure expansion, and also the contribution due to molecular heat conduction. We now define the turbulent Howarth variable R_T from the transformation

$$\rho_f R_T dR_T = \rho_f r dr \quad (14)$$

In the above, ρ_f is the mass density prevailing at the turbulent front.

From the semiempirical wake theory, we set⁽⁶⁾

$$\mathcal{E} = \kappa \left[u_f - u(0) \right] R_{Tf} \cdot d \quad (15)$$

From the approximate conservation of the stagnation enthalpy, we also have

$$\begin{aligned} h - h_{\infty} &= \frac{U_{\infty}^2 - u^2}{2} = \frac{(U_{\infty} - u)(U_{\infty} + u)}{2} \\ &\approx \left(\frac{1+f}{2} \right) U_{\infty} (U_{\infty} - u) \end{aligned} \quad (16)$$

Writing the above at $r = 0$ and $r = r_f$, we have

$$\left(\frac{1+f}{2}\right)[u_f - u(0)] U_\infty = h(0) - h_f \quad (17)$$

Substitution in Eq. (15) yields (for $j = 1$)

$$\frac{\mathcal{E}}{U_\infty d} = \kappa \frac{h_\infty}{\left(\frac{1+f}{2}\right) U_\infty^2} R_{Tf} \left[\frac{h(0) - h_f}{h_\infty} \right] \quad (18)$$

Now let the turbulent profile, assumed to be parabolic, be expressed as an excess of the enthalpy at the turbulent front by the equation

$$\frac{h - h_f}{h_\infty} = A(\bar{x}) B \left(\frac{R_T}{R_{Tf}} \right) \quad (19)$$

where

$$B \left(\frac{R_T}{R_{Tf}} \right) = 1 - \left(\frac{R_T}{R_{Tf}} \right)^2 \quad (20)$$

In the neighborhood of the axis we can set

$$\rho_f R_T^2 = \bar{\rho} \bar{r}^2 \quad (21)$$

We now use Eqs. (19) and (21) in Eq. (18) to calculate \mathcal{E} at the axis, since the equation of energy conservation will be satisfied in detail only there. The result is

$$\frac{\mathcal{E}}{U_\infty d} = \frac{\kappa h_\infty}{\left(\frac{1+f}{2}\right) U_\infty^2} \left[\frac{\rho(0)}{\rho_f} \right]^{1/2} A(\bar{x}) \bar{r}_f \quad (22)$$

The above was first derived in Ref. 3. At the axis, Eq. (13) yields, after introduction of the variable R_T , the diffusivity \mathcal{E} , and the approximation of Eq. (21), the following:

$$\frac{\partial \bar{h}}{\partial x} = \frac{4}{fU_\infty d} \left\{ \frac{\partial^2 \bar{h}}{\partial R_T^2} + \frac{1}{R_T} \frac{\partial \bar{h}}{\partial R_T} \right\} \mathcal{E} \quad (23)$$

The factor 4 in Eq. (23) enters because x is nondimensionalized with respect to the nose diameter d , whereas R is nondimensionalized with respect to r_0 .

The quantity in brackets above can be calculated easily from Eqs. (19) and (20). The result is

$$\frac{\partial \bar{h}}{\partial x} = \frac{-8A(\bar{x})}{fU_\infty d R_{Tf}^2} \mathcal{E} \quad (24)$$

In the neighborhood of $r = 0$ we have*

$$\rho_\infty R_f^2 \approx \rho_f R_{Tf}^2 \quad (25)$$

and hence

$$\frac{\partial \bar{h}}{\partial x} = - \frac{8A(\bar{x})}{fU_\infty d} \frac{\rho_f}{\rho_\infty} \frac{1}{R_f^2} \mathcal{E} \quad (26)$$

The left-hand side of this equation is now calculated at $r = 0$ with the help of Eq. (19)

*As shown in Ref. 3 from a conservation-of-mass argument, we have $R_f^2 - (\rho_f/\rho_\infty) R_{Tf}^2 = (\gamma - 1) M^2 C_{D_{fi}} / 8(1 + H)$. If we use Eq. (8), the quantity in the right-hand side is approximately equal to $(3/4) C_{D_{fi}}$, a very small quantity compared with the other terms except very close to the neck.

$$\frac{\partial \bar{h}}{\partial x} = \left(\frac{\partial \bar{h}}{\partial R_f} \right) \left(\frac{dR_f}{dx} \right) = \left\{ \frac{\partial \bar{h}_f}{\partial R_f} + \frac{\partial A(R_f)}{\partial R_f} \right\} \frac{dR_f}{dx} \quad (27)$$

Appendix B shows that it is legitimate to neglect the reduction of the inviscid enthalpy at the front due to the mechanism of molecular conduction, so that from Eq. (10) we obtain

$$\frac{\partial \bar{h}}{\partial x} = \left\{ - \frac{2HR_f}{C_D \left(1 + \frac{R_f^2}{C_D} \right)^2} + \frac{\partial A(R_f)}{\partial R_f} \right\} \frac{dR_f}{dx} \quad (28)$$

Before we can solve this equation for R_f , we need to evaluate the function $A(R_f)$. This is done in Appendix C, where a calculation is made of the amount of energy (or equivalent drag in terms of the local drag coefficient C_{Df}) contained within the turbulent core at a given station x . The total amount of energy (or total amount of drag) between $r = 0$ and $r = \infty$ remains, of course, constant along x , so that the difference in the drag of the turbulent core at two different axial stations is exactly equal to the difference of the energy (or drag) contained by the inviscid-energy profiles at the same two stations.* After some approximations in Appendix C, we obtain Eq. (C-7), which for convenience is combined here with Eq. (C-4).

$$A(R_f) = \frac{C_{Df} (\gamma - 1) M^2}{R_f^2} = \frac{(\gamma - 1) M^2}{\frac{R_{fi}^2}{C_{Dfi}} + \frac{R_f^2}{C_D}} \quad (29)$$

We now use in Eq. (24) the expressions for $A(R_f)$ and \bar{C} from Eqs. (29) and (22). After some algebra we find

*Uniform pressure is assumed in this argument.

$$\left\{ \frac{1}{6C_D \left(1 + \frac{R_f^2}{C_D}\right)^2} + \frac{1}{C_D \left(\frac{R_{fi}^2}{C_{D_{fi}}} + \frac{R_f^2}{C_D}\right)^2} \right\} \frac{dR_f}{dx} = \frac{4k \sqrt{\frac{\rho(0)}{\rho_\infty}}}{\left(\frac{1+f}{2}\right) f R^2 \left(\frac{R_{fi}^2}{C_{D_{fi}}} + \frac{R_f^2}{C_D}\right)^2} \quad (30)$$

We now calculate the density ratio $\rho(0)/\rho_\infty$ by assuming an ideal gas and using Eqs. (10)* and (29)

$$\begin{aligned} \frac{\rho_\infty}{\rho(0)} &= \frac{h(0)}{h_\infty} \cdot \frac{p_\infty}{p(0)} = \left\{ 1 + \frac{h_f}{h_\infty} + A(R_f) \right\} \frac{p_\infty}{p(0)} \\ &= \left\{ 1 + \frac{H}{\left(1 + \frac{R_f^2}{C_D}\right)} + \frac{(\gamma - 1)M^2}{\left(\frac{R_{fi}^2}{C_{D_{fi}}} + \frac{R_f^2}{C_D}\right)} \right\} \frac{p_\infty}{p(0)} \end{aligned} \quad (31)$$

Substitution of the above in Eq. (30) yields, after some rearrangement and integration

$$\begin{aligned} \int \frac{R_f^2}{C_D} \left[6 + \frac{\left(\frac{R_{fi}^2}{C_{D_{fi}}} + \frac{R_f^2}{C_D}\right)^2}{1 + \frac{R_f^2}{C_D}} \right] \sqrt{1 + H \left[\frac{1}{\left(1 + \frac{R_f^2}{C_D}\right)} + \frac{6}{\left(\frac{R_{fi}^2}{C_{D_{fi}}} + \frac{R_f^2}{C_D}\right)} \right]} \frac{dR_f}{\sqrt{C_D}} \\ = \frac{24K}{\left(\frac{1+f}{2}\right) f \sqrt{C_D}} \int \sqrt{\frac{\rho(0)}{\rho_\infty}} d\bar{x} + (\text{const}) \end{aligned} \quad (32)$$

This equation gives the growth of the turbulent core in the Howarth

* In this step we add one to the right-hand side of Eq. (10) in order to make it an exact equation as $R \rightarrow \infty$, since the density ratio must be accurate for both small and large R .

plane. In Appendix D, by using the ideal gas law, we calculate R_f as a function of the physical co-ordinate \bar{r}_f after using Eq. (10). The result, repeated here, is

$$\bar{r}_f^2 = \frac{p_\infty}{p(0)} \left[R_f^2 + C_D H \ln \left(1 + \frac{R_f^2}{C_D} \right) \right] \quad (33)$$

Now the function $\bar{r}_f(\bar{x})$ could be calculated if we knew the quantities $p(0)/p_\infty$, the constant of integration, κ , and $R_{fi}^2/C_{D_{fi}}$.

As has been mentioned before, the pressure ratio $p(0)/p_\infty$ can only be given by solving exactly the interaction problem of the trailing shock with the wake core. Since such a solution is not available, the approximations of Ref. 3 described in the Introduction of this Memorandum are appropriate. The constant of integration appearing in Eq. (32) can be set equal to a value giving the position of the neck and its thickness as observed in experiments; this was also the procedure adopted in Ref. 3. It is obvious that the value of this constant has an influence only a very few diameters downstream from the neck.

The value of κ is again offered as an additional arbitrary parameter, but the remarkable thing is (as mentioned in Ref. 3) that experimental evidence suggests the same value used in subsonic wakes. This value is approximately equal to 0.035.

Finally, an estimate must be made of the quantity $R_{fi}^2/C_{D_{fi}}$. From Eq. (29), recalling the definition for $A(\bar{x})$ from Eq. (19), we find

$$\frac{R_{fi}^2}{C_{D_{fi}}} = \frac{(\gamma - 1)M^2}{\frac{h_i(0) - h_{fi}}{h_\infty}} \quad (34)$$

For the ratio h_{fi}/h_∞ we may use the value h_{x_0}/h_∞ , given by Eq. (10), since initially we are very close to the axis.

An exact computation of the ratio $h_1(0)/h_\infty$ is not possible, since the near-wake problem remains unsolved. However, the physical description of Ref. 7 could be used as a guide. If we assume that the "dividing streamline" brings the fluid to rest just at the center of the neck, the enthalpy for an insulated body will be approximately equal to the stagnation enthalpy (for Prandtl number of order one). If heat transfer is allowed at the body, then this enthalpy will be smaller.

Now let λ be the fraction of the stagnation enthalpy* to which $h_1(0)/h_\infty$ is equal. For the reason explained above we shall treat λ as an additional free parameter. The ratio $R_{fi}^2/C_{D_{fi}}$ depends on λ only and can be calculated from Eq. (34) after use is made of Eq. (8):

$$\frac{R_{fi}^2}{C_{D_{fi}}} \approx \frac{1}{\frac{\lambda}{2} - \frac{1}{6}} \quad (35)$$

For the values of $R_{fi}^2/C_{D_{fi}} = 3, 4, 6, 8, 10$, and 12 , the corresponding λ 's = $1.0, 0.83, 0.67, 0.58, 0.53$, and 0.50 .

We proceed now to examine the asymptotic character of Eq. (32) for small and large distances downstream. It is easy to establish that for small values of R_f , Eq. (32) gives

$$R_f^3 \left[\left(\frac{R_{fi}^2}{C_{D_{fi}}} \right)^2 \sqrt{1+H} \right] \approx \frac{72\kappa C_D}{\left(\frac{1+f}{2} \right)_f} \int \sqrt{\frac{p(0)}{p_\infty}} d\bar{x} + (\text{const}) \quad (36)$$

If we approximate Eq. (33) for small R_f 's and use Eqs. (8) and (35), the above becomes

$$\bar{r}_f^3 \approx \frac{12\kappa C_D}{\left(\frac{1+f}{2} \right)_f} (\gamma - 1)M^2 \left(\frac{\lambda}{2} - \frac{1}{6} \right)^2 \int \sqrt{\frac{p_\infty}{p(0)}} d\bar{x} + (\text{const}) \quad (37)$$

*The stagnation enthalpy is equal to $h_{st}/h_\infty \approx (\gamma - 1)M^2/2 \approx 3H$.

At high values of R_f , when the influence of the parameter $R_{fi}^2/C_{D_{fi}}$ ceases to exist, Eq. (32) becomes

$$r_f^3 \approx \frac{12\kappa C_D}{\left(\frac{1+f}{2}\right)_f} \bar{x} \quad (38)$$

It is thus concluded that the value of $R_{fi}^2/C_{D_{fi}}$ and H (and hence the Mach number) is only significant during the initial period of the process. Very far downstream, only the drag C_D (essentially equal to the total drag, since $C_{D_{fi}}$ is so small) affects the growth of the wake, exactly as in the subsonic case. For all the cases studied, this distance is of the order of 1000 diameters downstream. In a log-log presentation, the straight line of Eq. (37) can assume a higher or lower position relative to Eq. (38). The position will be higher at the higher Mach numbers and higher values of λ (no heat-transfer effects), as one would expect on physical grounds.

The function $\bar{r}_f(\bar{x}, R_{fi}^2/C_{D_{fi}})$ for $M = 8.5$ is plotted in Fig. 3 for the several values of λ , along with the experimental data of Ref. 8. It is seen that the influence of the factor λ is limited at high \bar{x} , and certainly an exact value for λ or $R_{fi}^2/C_{D_{fi}}$ cannot be decided from the experiments, since the scatter is high at the smaller \bar{x} 's where the influence of λ is stronger. For Fig. 3, the constant of integration of Eq. (32) was set equal to zero. Given a set of values of $C_{D_{fi}}$ and λ , the quantity R_{fi} is fixed, and hence so is \bar{r}_{fi} . For different values of $C_{D_{fi}}$ but fixed λ 's we will have different \bar{r}_{fi} 's, which, however, should physically correspond to the same \bar{x}_i . The value of \bar{x}_i should be selected from experimental observation, and the constant of integration accordingly fixed so that the curve goes through the point \bar{r}_{fi}, \bar{x}_i . This procedure amounts to an appropriate sliding of the co-ordinate \bar{x} by a constant (positive or negative) value. In Fig. 3 the curve obtained in Ref. 3 allowing for pressure variation is shown, along with another one in which the pressure was

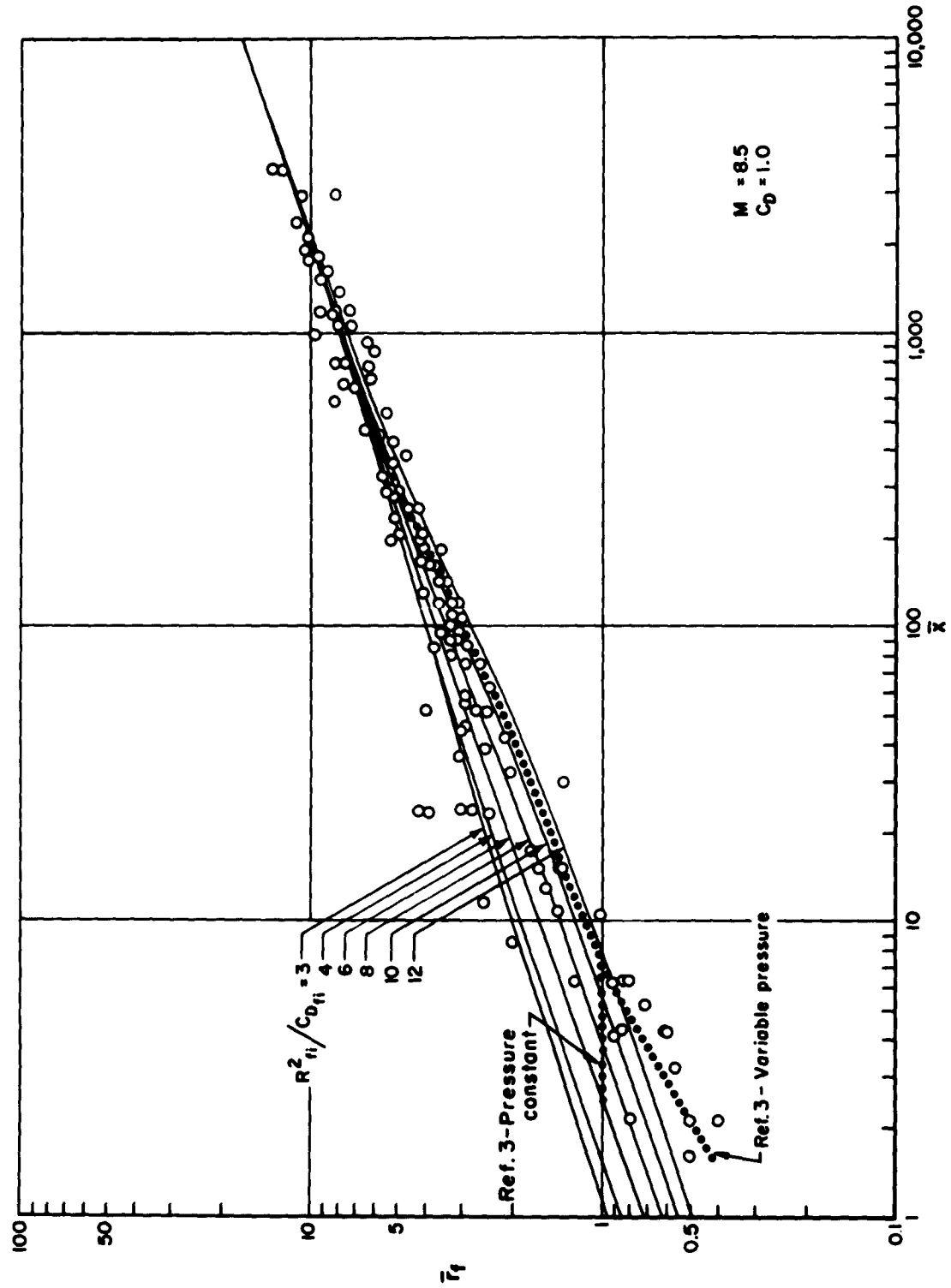


Fig. 3 — Comparison of the growth of the turbulent core of a blunt body with $C_D=1.0$ and several $R_{ti}^2/C_{D_{ti}}$ values according to present theory (constant pressure) with theory of Ref. 3 and the experimental data of Ref. 8 for $M=8.5$

kept constant everywhere. It should be noted that the curves of Fig. 3 obtained in Ref. 3 correspond to the value $R_{fi}^2/C_{D_{fi}} \approx 10$; it is seen that the agreement with Eq. (32) is very good.

In Fig. 4 the function $\bar{r}_f(\bar{x})$ is shown plotted for different values for $R_{fi}^2/C_{D_{fi}}$ and $M = 22$. Here again the constant of integration in Eq. (32) is set equal to zero. In the same figure the curves calculated for constant and variable pressure are shown.⁽³⁾ The quantity $R_{fi}^2/C_{D_{fi}}$ was taken in Ref. 3 to be equal to about 11. It is apparent that even when adjustment is made for the curve corresponding to $R_{fi}^2/C_{D_{fi}} = 10$ or 12 to pass through the point $\bar{x} = 7.5$ and $\bar{r}_f = 1.8$, the agreement with Ref. 3 is not as good in the present case as it was for the case $M = 8.5$. It should be noted, however, that the general trend of the curve $\bar{r}_f(\bar{x})$ is the same as the one of Ref. 3. The numerical differences (certainly small when considering the scatter of the usual experimental data obtained in the ballistic range and the crude character of the semiempirical turbulent theory used) are due to the fact that the function $\bar{r}_f(\bar{x})$ depends on the slopes of both functions \bar{h}_f and A , as can be seen from Eq. (27). Since both \bar{h}_f and A (Eqs. (10) and (29)) provide inflection points, differences are to be expected when comparing results with other analytical representations of these curves, which are in good agreement in the ordinates but have significant differences in the slopes.

In Fig. 5 a plot similar to Figs. 3 and 4 is shown for $M = 16$.

Observation of Figs. 3, 4, and 5 shows that for small and very high \bar{x} the turbulent core (pressure variation apart) grows with the $1/3$ power of \bar{x} according to Eqs. (37) and (38). In Fig. 6 the value of the quantity $R_{fi}^2/C_{D_{fi}}$ is kept constant (equal to 10), and the curve $\bar{r}_f(\bar{x})$ is plotted for Mach numbers equal to 8.5, 16, and 22. The pressure has been kept constant, and the constant of integration of Eq. (32) has been set equal to zero. Note that the influence of the cooling by expansion is stronger for the high Mach numbers (and is present also over longer distances downstream).

In Appendix E, Figs. E-1 through E-6 give the function $\bar{r}_f(\bar{x})$ for several Mach numbers and values of the parameter $R_{fi}^2/C_{D_{fi}}$.

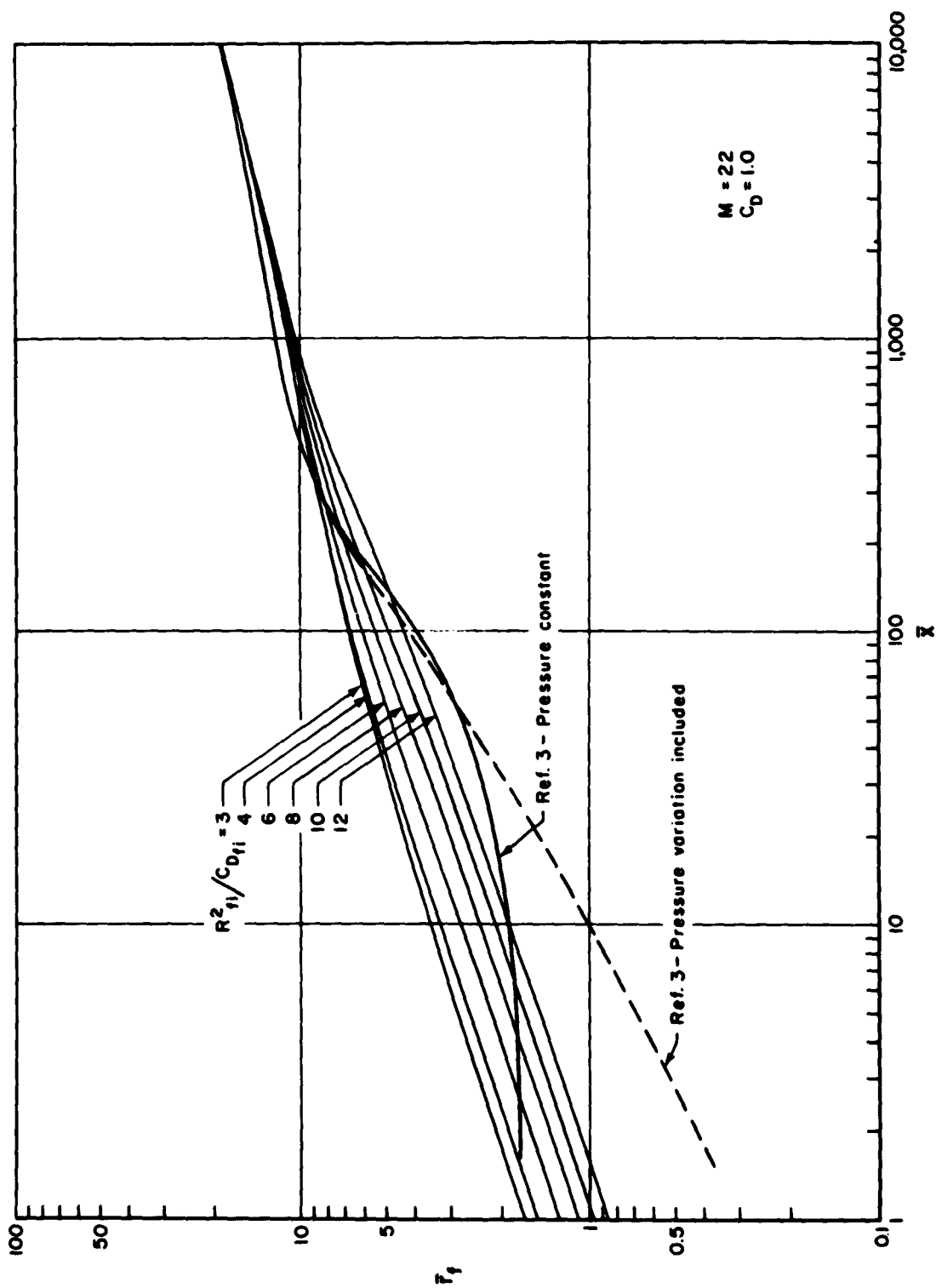


Fig. 4 — Comparison of the growth of the turbulent core of a blunt body with $C_D = 1.0$ and several R^2_{f1}/C_{Df1} values according to present theory (constant pressure) with theory of Ref. 3 for $M = 22$

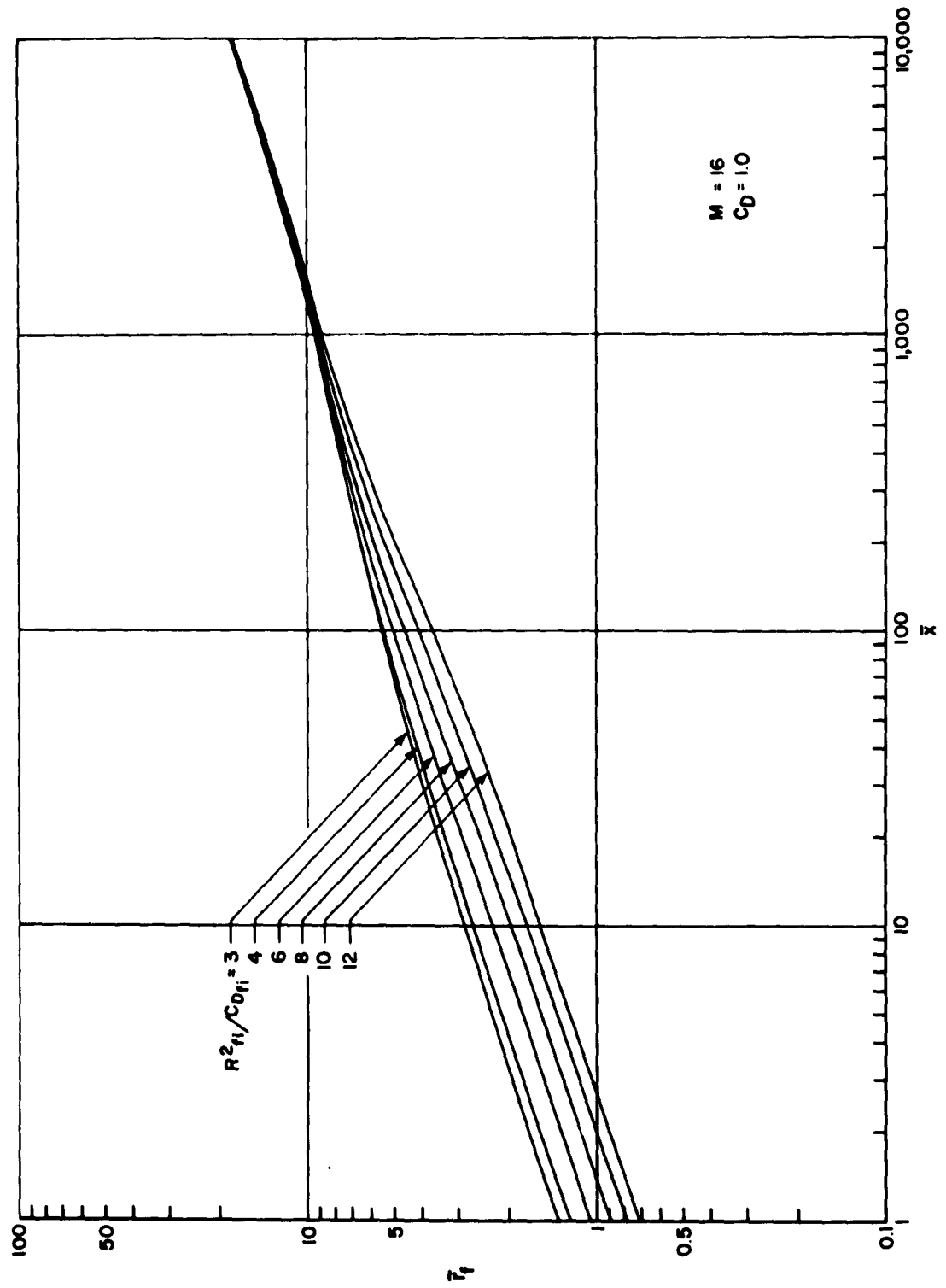


Fig. 5 — The growth of the turbulent core assuming constant pressure for $C_D = 1.0$, $M = 16$, and several $R^2_{fi}/C_{D_{fi}}$ values

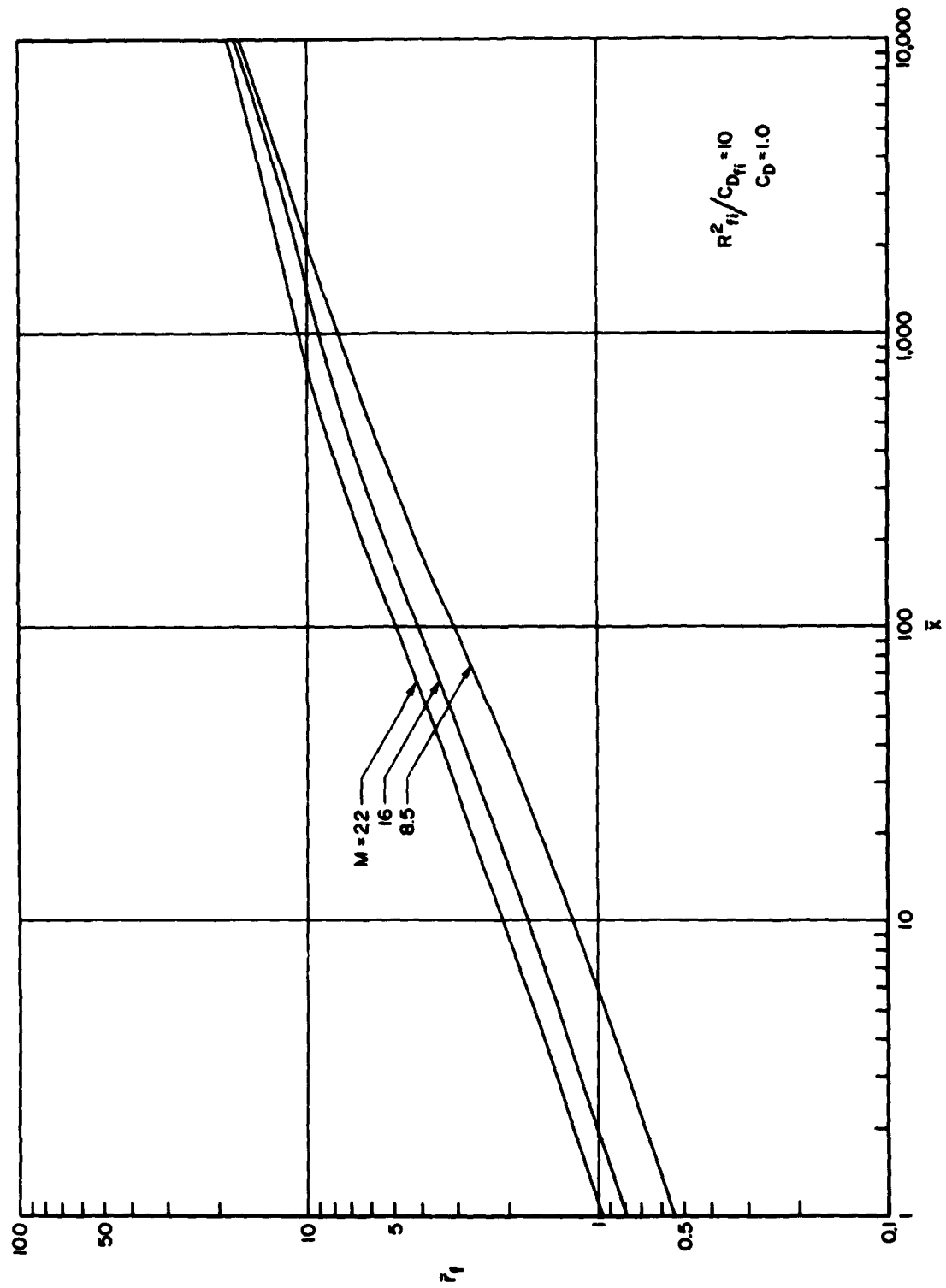


Fig. 6 — The growth of the turbulent core assuming constant pressure for $C_D = 1.0$, $R^2_{ti}/C_{D_{ti}} = 10$, and different Mach numbers

III. ANALYSIS FOR THE CASE OF CONES AND SLENDER BODIES

The basic difference between the case of the turbulent wake behind a blunt body, such as analyzed in the previous section, and that of a slender one is that in the first geometry, high temperatures are developed at the stagnation point where the flow comes to rest by hitting the wall perpendicularly, whereas in the second, high temperatures are developed in the boundary layer where the flow comes to rest through the action of the viscous forces which act parallel to the wall. In the case of blunt bodies it was found that most of the momentum deficiency was located in the inviscid flow through the action of the shock wave, with high characteristic enthalpies prevailing at the cross section $x = x_0$ equal to about $1/3$ the stagnation enthalpy ($H \approx (\gamma - 1)M^2/6 \sim H_{st}/3$). The distribution of the drag at the neck was such that $C_D \gg C_{D_{fi}}$. Consider now as an extreme the case of a thin cone. Even at high Mach numbers the oblique shock wave formed at the tip decelerates the flow very little, and hence the inviscid enthalpies are very low compared with the enthalpies prevailing inside the boundary layer or at the neck.

Figure 7 shows schematically the relative position at the neck of the enthalpy profiles for the viscid and inviscid parts of the two cases under discussion. The inviscid solutions are for an infinite thin cone and a hemisphere-cylinder and are modified at the neck by two parabolic profiles. The case of a blunted cone will lie somewhere between the curves for a pure cone and hemisphere-cylinder. As pointed out in Ref. 9, the shock wave in the neighborhood of the tip is given reasonably well by the cylindrical blast-wave theory based on the curvature of the nose, whereas far from the body the same is true if the radius of the base is taken into consideration. The region in between is approximated by a conical shock which allows for a slight recompressibility zone. The exact shape of the shock wave is needed for the determination of the enthalpy profile at the cross section $x = x_0$ where the pressure is almost ambient. In the fashion of Ref. 1 this distribution can be obtained in terms of the shock

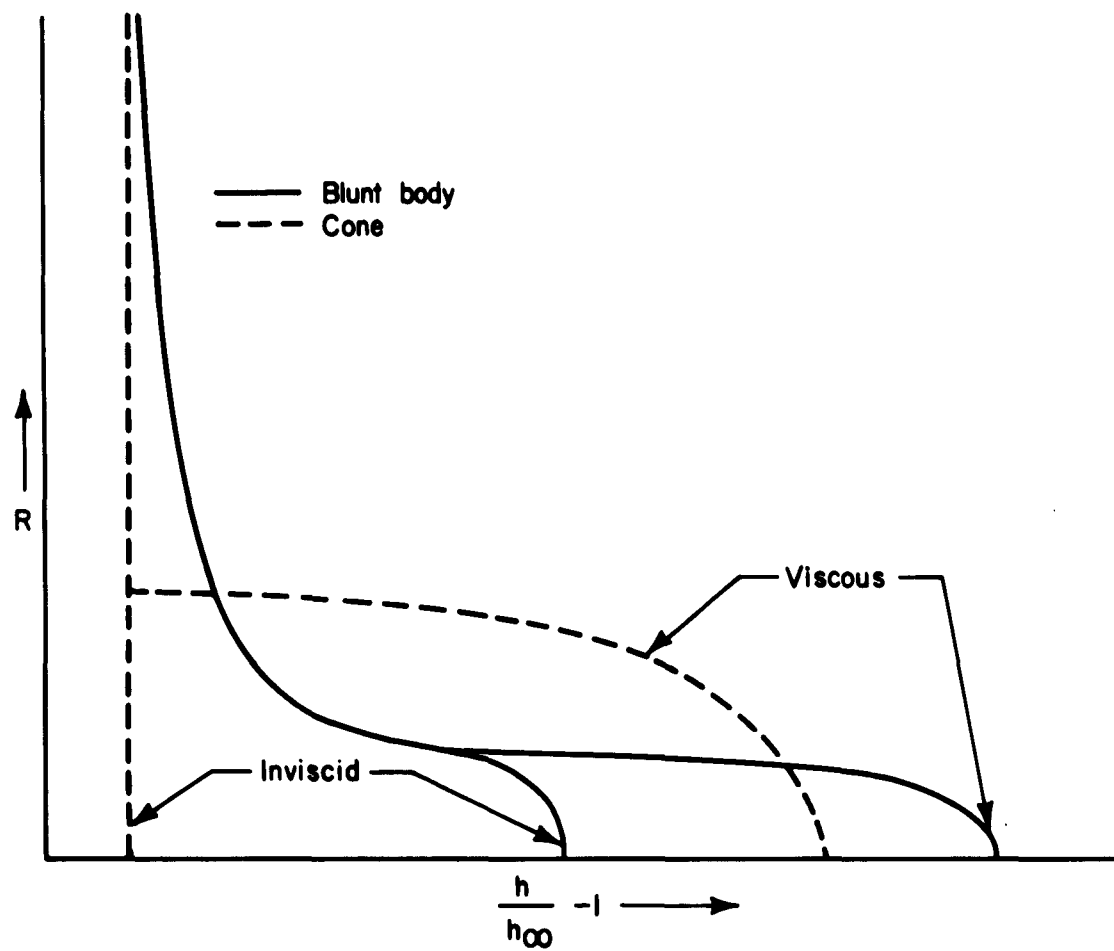


Fig. 7 — Schematic enthalpy distribution at the neck in the wake of a blunt body and a thin cone for the same Mach number

angle β by using the regular conditions across the shock wave and expanding isentropically along each different-entropy streamline. This procedure yields

$$\frac{h_{x_0}(R)}{h_\infty} = \frac{1 + \left(\frac{\gamma-1}{2}\right) M^2 \sin^2 \beta}{\left[\left(\frac{2\gamma}{\gamma+1}\right) M^2 \sin^2 \beta - \frac{\gamma-1}{\gamma+1}\right]^{1-\frac{1}{\gamma_L}}} \quad (39)$$

where

$$\sin^2 \beta = \left[1 + (dR_s/dx)^{-2}\right]^{-1} \quad (40)$$

The term γ_L is an effective specific-heat ratio which accounts for real gas effects. For blunt bodies, γ_L was found to be approximately equal to 1.2 in Ref. 1. For thin, slender cones, γ_L should approach the value 1.4, since the temperatures for this case are lower by far. The distance $x = x_0$ is located where the angle of the shock wave becomes the Mach angle, or

$$\sin^2 \beta_0 = \frac{1}{1 + \frac{1}{(dR_s/dx)^2}} = \frac{1}{M^2} \quad (41)$$

Equation (41) is an exact one, valid for both thin and blunt bodies but not for infinite cones.*

We now write the energy equation (Eq. (13)) without making specific substitutions for the functions \bar{h}_f and A . We have

$$\frac{R_f}{A^2} \left[\frac{\partial \bar{h}_f}{\partial R_f} + \frac{dA}{dR_f} \right] \sqrt{(1 + \bar{h}_f + A) \frac{p_\infty}{p(0)}} dR_f = \frac{-8\kappa d\bar{x}}{f \left(\frac{1+f}{2}\right) (\gamma-1) M^2} \quad (42)$$

The term \bar{h}_f can be obtained from Eq. (39) by making $R = R_f$. On

*A finite cone will have a shock wave bent towards the center line by virtue of the interaction with the expansion fan.

the other hand, the expression for $A(R_f)$ found in Appendix C needs no modification except that now the approximation $C_D \gg C_{D_{fi}}$ is not valid, and as a consequence Eq. (C-6) must be used. This equation is reproduced below for continuity after combination with Eq. (29):

$$A = \frac{C_{D_f} (\gamma - 1) M^2}{R_f^2} = \frac{(\gamma - 1) M^2}{R_{fi}^2 \left(\frac{1}{C_{D_{fi}}} - \frac{1}{C_D} \right) + \frac{R_f^2}{C_D}} \quad (43)$$

Equation (42) can now be integrated by using Eqs. (39) and (40) for the determination of \bar{h}_f , and Eq. (43) for the function A.

Let us now consider as an example the case for which $M^2 \sin^2 \beta$ is a large number in order for the following approximation of Eq. (39) to be permissible: (see Appendix F for a detailed discussion of this assumption)

$$\frac{h_{x_o}(R)}{h_\infty} = \left(\frac{\gamma - 1}{2} \right) \left(\frac{\gamma + 1}{2\gamma} \right)^{\left(1 - \frac{1}{\gamma_L} \right)} \left[\frac{M^2}{1 + (dR_s/dx)^{-2}} \right]^{\frac{1}{\gamma_L}}$$

We may neglect for convenience the quantity in the second parenthesis, so that

$$\frac{h_{x_o}(R)}{h_\infty} = \left(\frac{\gamma - 1}{2} \right) \left[\frac{M^2}{1 + (dR_s/dx)^{-2}} \right]^{\frac{1}{\gamma_L}} \quad (44)$$

As in the case of the blunt body let us set

$$\frac{h_{x_o}(R)}{h_\infty} = 1 + \frac{H}{\left[1 + (R'_s)^{-2} \right]^{1/\gamma_L}} \quad (45)$$

The prime indicates differentiation with respect to the co-ordinate of the shock wave x , not to be confused with the distance downstream from the neck over which we study the growth of the turbulent core.

Differentiation of Eqs. (43) and (45) and substitution in Eq. (42) yield, after some algebra

$$\begin{aligned}
 R_f^2 & \left\{ 1 - \frac{H C_D \left\{ R_{fi}^2 \left(\frac{1}{C_{Dfi}} - \frac{1}{C_D} \right) + \frac{R_f^2}{C_D} \right\}^2 R_s''}{\gamma_L (\gamma - 1) M^2 (1 + R_s'^2) \left(1 + \frac{1}{\gamma_L} \right) R_s'^2 \left(1 - \frac{1}{\gamma_L} \right) R_f} \right\} \\
 & \times \sqrt{1 + \frac{H}{\left[1 + (R_s')^{-2} \right]^{1/\gamma_L}} + \frac{(\gamma - 1) M^2}{R_{fi}^2 \left(\frac{1}{C_{Dfi}} - \frac{1}{C_D} \right) + \frac{R_f^2}{C_D}}} dR_f \\
 & = \frac{4 \kappa C_D}{f \left(\frac{1+f}{2} \right)} \sqrt{\frac{p(0)}{p(\infty)}} d\bar{x} \quad (46)
 \end{aligned}$$

From the above we see clearly the strong dependence of the growth of the turbulent core on the second derivative (or curvature) of the shape of the shock wave.

As a limiting case we further study in some detail the case of a pure cone in the approximation $M^2 \sin^2 \theta \gg 1$. In this case we set the factor $f \approx 1$, and from Eq. (4) we see that R_s is exactly equal to the Howarth variable R . Also, if θ is the angle of the cone (assumed small), we have for the shape of the shock

$$R_s = R \approx \left(\frac{\gamma + 1}{2} \right) \theta \bar{x} \quad (47)$$

From Eq. (44) we also find

$$H = \left(\frac{\gamma - 1}{2} \right) \left[M \left(\frac{\gamma + 1}{2} \right) \theta \right]^{2/\gamma_L} \quad (48)$$

Equation (42) becomes

$$R_f^2 \left\{ 1 + \frac{\left(\frac{\gamma - 1}{2} \right) \left[M \left(\frac{\gamma + 1}{2} \right) \theta \right]^{2/\gamma_L}}{\left\{ 1 + \left[\left(\frac{\gamma + 1}{2} \right) \theta \right]^2 \right\}^{2/\gamma_L}} + \frac{(\gamma - 1)M^2}{R_{fi}^2 \left(\frac{1}{C_{D_{fi}}} - \frac{1}{C_D} \right) + \frac{R_f^2}{C_D}} \right\}^{1/2} dR_f$$

$$= 4\kappa C_D \sqrt{\frac{p(0)}{p_\infty}} d\bar{x} \quad (49)$$

The second expression under the radical on the left-hand side, representing the inviscid effects, is negligibly small for small θ compared with the third part, which contains the strong viscous effects. We now integrate Eq. (49) in the limiting case of small \bar{x} . We distinguish the following cases:

A. Let us assume that $C_{D_{fi}} = C_{D_f} = C_D$.

This is the case of very thin cones (a few degrees half angle) and small Reynolds numbers. Pressure variation apart, Eq. (49) yields after integration

$$\frac{R_f^2}{C_D} = \frac{8\kappa}{\sqrt{(\gamma - 1)M^2 C_D}} (\bar{x} - \bar{x}_i) + \frac{R_{fi}^2}{C_D} \quad (50)$$

B. Let $C_{D_{fi}} \ll C_D \ll 1.0$.

In this case the denominator of the last part under the radical is approximated by $R_{fi}^2/C_{D_{fi}}$. After integration we have

$$\frac{R_f^2}{C_D} = \left\{ \frac{12\kappa}{\sqrt{(\gamma - 1)M^2 C_D}} \frac{R_{fi}^2}{C_{D_{fi}}} (\bar{x} - \bar{x}_i) + \frac{R_{fi}^3}{C_D^{3/2}} \right\}^{2/3} \quad (51)$$

For completeness and for the benefit of ready comparison we give below the equivalent result for blunt bodies (Eq. (36)). We assume $(1 + f)/2f \approx 1.0$, but we incorporate the pressure term in an average sense, since for blunt bodies, especially at high Mach numbers, it is significant.

$$\frac{R_f^2}{C_D} = \left\{ \frac{72\kappa}{(R_{fi}^2/C_{D_{fi}})^2 \sqrt{(\gamma - 1)M^2 C_D}} \left[\frac{p(0)}{p_\infty} \right]_{\text{avg}}^{1/2} (\bar{x} - \bar{x}_i) + \frac{R_{fi}^3}{C_D^{3/2}} \right\}^{2/3} \quad (52)$$

The decay of the enthalpy along the axis is given by Eq. (19) as follows:

$$\frac{h(0)}{h_\infty} = \frac{h_f}{h_\infty} + A = \frac{\left(\frac{\gamma - 1}{2} \right) \left[M \left(\frac{\gamma + 1}{2} \right) \Theta \right]^{2/\gamma_L}}{\left\{ 1 + \left[\left(\frac{\gamma + 1}{2} \right) \Theta \right]^2 \right\}^{1/\gamma_L}} + \frac{(\gamma - 1)M^2}{R_{fi}^2 \left(\frac{1}{C_{D_{fi}}} - \frac{1}{C_D} \right) + \frac{R_f^2}{C_D}} \quad (53)$$

The equivalent result for a blunt body is

$$\frac{h(0)}{h_\infty} = \frac{(\gamma - 1)M^2}{6 \left(1 + \frac{R_f^2}{C_D} \right)} + \frac{(\gamma - 1)M^2}{\frac{R_{fi}^2}{C_{D_{fi}}} + \frac{R_f^2}{C_D}} \quad (54)$$

From Eq. (53) we see that in the case of a pure cone the part of the

enthalpy due to the shock wave is negligibly small compared to the part due to the viscous effects. From Eq. (54) we see that for small \bar{x} the reverse is true for blunt bodies.

We now examine the quantity $R_{fi}^2/C_{D_{fi}}$ in the case of cones. From Eq. (34), valid for all cases, we note that $h_1(o) \gg h_{fi}$, and hence Eq. (34) reduces in terms of the parameter λ to

$$\frac{R_{fi}^2}{C_{D_{fi}}} = \frac{2}{\lambda} \quad (55)$$

Bearing the above in mind, we use Eqs. (50), (51), and (55) in Eq. (53), and Eqs. (35) and (52) in Eq. (54); we find the following:

For the case of a cone with $C_{D_{fi}} = C_D \ll 1$ and for small \bar{x}

$$\frac{h(o)}{h_\infty} = \frac{(\gamma - 1)M^2}{\frac{2}{\lambda} + \frac{8\kappa}{\sqrt{(\gamma - 1)M^2 C_{D_{fi}}}} (\bar{x} - \bar{x}_1)} \quad (56)$$

For the case of a cone with $C_{D_{fi}} \ll C_D \ll 1$ and for small \bar{x}

$$\frac{h(o)}{h_\infty} = \frac{(\gamma - 1)M^2}{\frac{2}{\lambda} \left[1 - \frac{C_{D_{fi}}}{C_D} \right] + \left\{ \frac{12\kappa}{\sqrt{(\gamma - 1)M^2 C_D}} \sqrt{\frac{2}{\lambda}} (\bar{x} - \bar{x}_1) + \left(\frac{2}{\lambda} \frac{C_{D_{fi}}}{C_D} \right)^{3/2} \right\}^{2/3}} \quad (57)$$

For the case of a blunt body with $C_{D_{fi}} \ll C_D \approx 1.0$

$$\frac{h(o)}{h_\infty} = \left(\frac{3\lambda - 1}{6} \right) (\gamma - 1) M^2$$

$$+ \frac{(\gamma - 1) M^2}{6 + \left\{ \frac{72(3\lambda - 1)^2 \kappa}{\sqrt{(\gamma - 1) M^2 C_D}} \left[\frac{p(o)}{p_\infty} \right]^{1/2} (\bar{x} - \bar{x}_1) + \left(\frac{36}{3\lambda - 1} \frac{C_{D_{fi}}}{C_D} \right)^{3/2} \right\}^{2/3}} \quad (58)$$

The following conclusions can now be drawn from the above equations:

1. The level of the initial enthalpy at the neck is of the same order for both blunt and slender bodies, since at the neck there is a tendency for the stagnation enthalpy to be recovered at the point where the dividing stream line of the free shear layer crosses the axis.

2. In the cases of cones or blunt bodies, the smaller the amount of total drag, the higher the decay of the enthalpy, as one would expect intuitively. This is shown by the fact that the factor which multiplies $(\bar{x} - \bar{x}_1)$ in Eqs. (56), (57), and (58) increases with smaller C_D .

3. Comparison of Eqs. (57) and (58), representing the most usual cases in practice, shows that for the same M , λ , and $C_{D_{fi}}$ the enthalpy decays faster for a cone with $C_D \ll 1.0$. Examination of the quantities multiplying $(\bar{x} - \bar{x}_1)$ in Eqs. (57) and (58) shows that their ratio (for a value $\lambda = 1/2$) is equal to

$$\frac{4}{3} \sqrt{\frac{(C_D)_b}{(C_D)_c} \left[\frac{p_\infty}{p(o)} \right]_{\text{avg}}}$$

where the subscripts b and c stand for the blunt and conical bodies; the pressure term refers to the blunt case, since for thin cones, cooling by expansion is not significant. One can see that the pressure cooling for the blunt bodies competes with the reduced drag mechanism for slender bodies, especially at the high Mach numbers. From Ref. 4

at $M = 22$ we estimate $(p(o)/p_\infty)_{avg} \approx 10$ and we see that even for $(C_D)_c = 0.1$ the quantity multiplying $(\bar{x} - \bar{x}_i)$ in the conical case will be a little higher when compared to the blunt case. On the other hand one can see again by observing Eqs. (57) and (58) that the expression containing \bar{x} in the braces in Eq. (57) dominates faster the number to its left, since this number is smaller than 6 (which corresponds to the blunt case) as long as $\lambda > 1/3$.^{*} The above effects are shown qualitatively in Fig. 8.

For the case of a blunted cone, the inviscid enthalpy distribution will look qualitatively as shown in Fig. 9, due to the fact that the flow suffers a recompression in the conical part of the shock.⁽⁹⁾ Since inflection points influence the growth of the turbulent core (see Eq. (46)), through the second derivative R_g'' , the growth curve $\bar{r}_f(\bar{x})$ will contain a number of wiggles depending on the relative position of the "viscous" parabolic profile with respect to the inviscid one. It might be instructive to compare a spherically blunted cone and a pure cone having the same total drag coefficient and flying at the same altitude and Mach number. For the reasons explained above, we expect the growth curve $\bar{r}_f(\bar{x})$ of the blunted cone to exhibit irregularities due to over-expansions and recompressions. Eventually, at high distances \bar{x} , when the wake behaves like an incompressible one, both curves will tend asymptotically toward the same straight line in the log-log representation. This effect is shown in Fig. 10. On the other hand, it is easy to see from Eq. (52) that the decay of the enthalpy at the axis will be slower for the blunted cone in the initial stages than for the pure cone, resuming the same rate later on when the compressibility effects are again absent. Numerical solutions for several conical geometries are reported in Ref. 12.

^{*}This has been tacitly assumed in writing Eq. (35); physically it means that the enthalpy at the neck must be higher than the enthalpy at the cross section where the pressure is ambient.

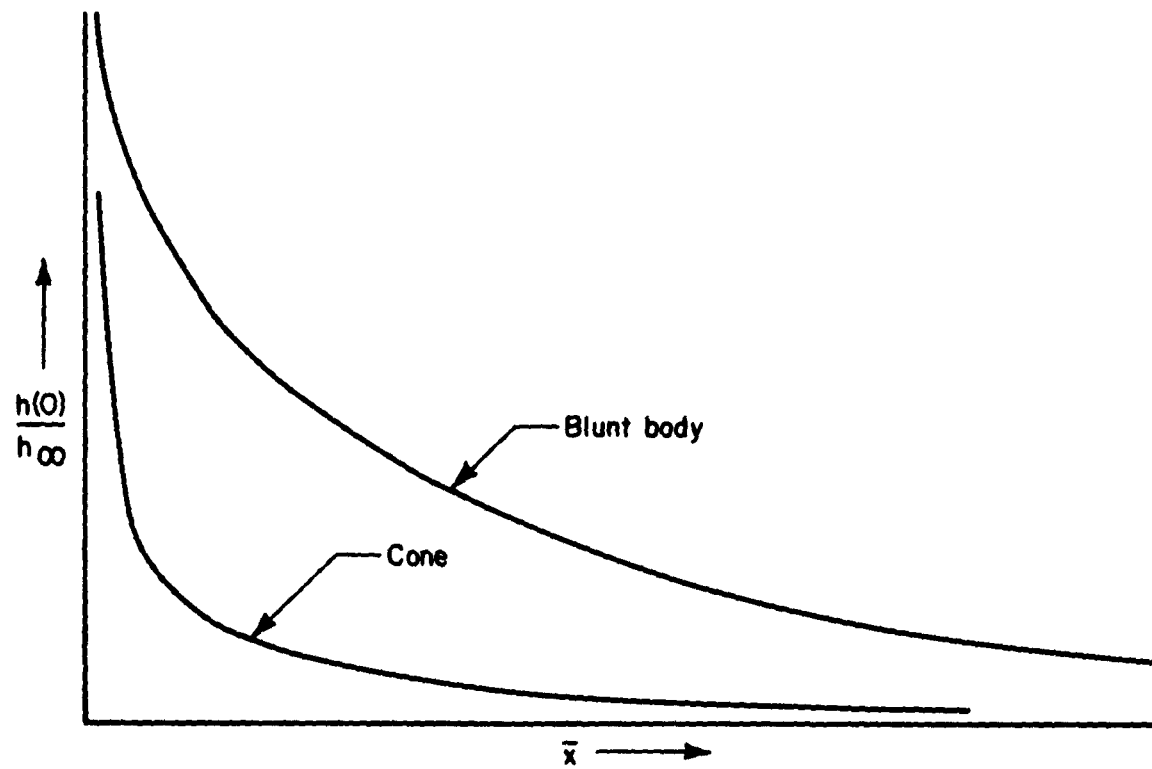


Fig. 8 — Schematic decay of the enthalpy at the axis of a wake behind a blunt body and a cone for the same Mach number

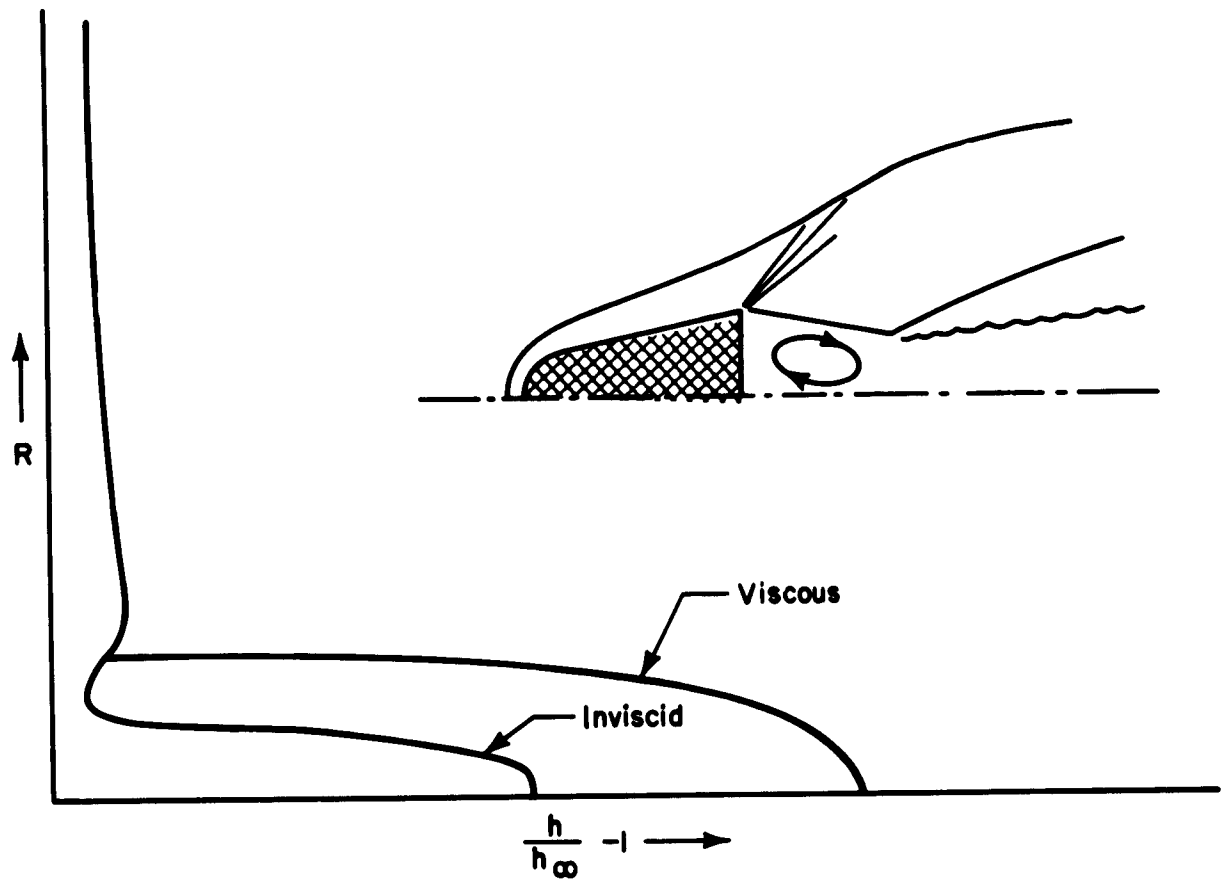


Fig. 9 — Schematic enthalpy profile at the neck in the wake of a blunted cone

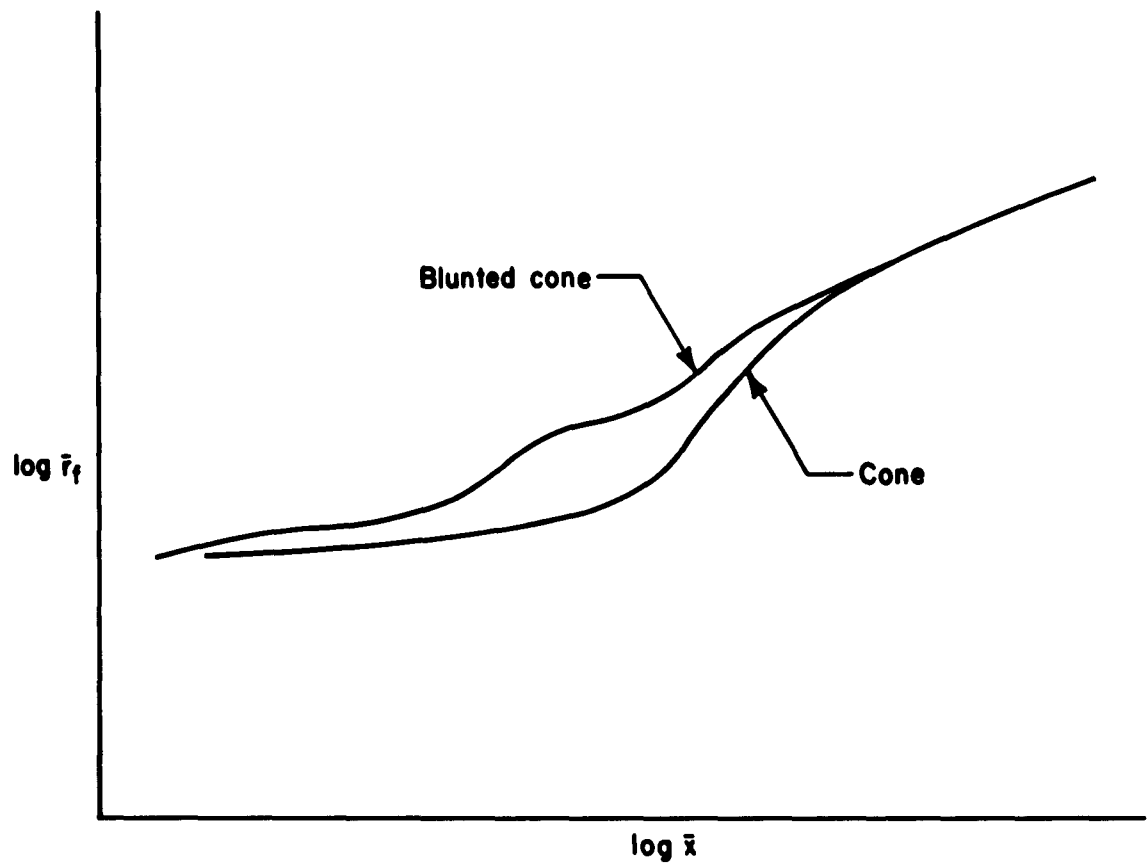


Fig.10— Schematic shape and relative growth of the turbulent core behind a blunted cone and a cone of the same total drag coefficient for the same Mach number

IV. CONCLUSIONS

An attempt was made to study the growth of the turbulent core in the wake behind blunt and slender bodies flying at hypersonic speeds. An exact analysis is not possible because of incomplete understanding of the following: (a) the flow in the near wake and the neck where a recompression occurs through the trailing shock; (b) the mechanism of transition to turbulence; (c) the structure of fully established turbulent flow in a compressible wake.

In order to compensate for problem (a) above, we treat the quantity of the enthalpy at the center of the neck as an additional parameter, and we proceed to study its effect. Problem (b) is more serious. In the present work we assume that fully established turbulence starts at the neck. Evidence from ballistic-range experiments⁽¹⁰⁾ suggests that this is the case at the higher densities, whereas at lower densities the transition point (roughly defined by the distance where the intermittency region appears) could appear many diameters downstream. The theory presented here can easily be modified to take into account this last effect, provided that the initial conditions from the point where the turbulent flow is fully established are known. For problem (c), the best that can be done is to extend our semiempirical knowledge on the subsonic wakes to the hypersonic case as suggested in Ref. 3. Only detailed comparison of many of the quantities predicted by the theory will show to what extent this procedure is correct. It must be admitted that the growth of the turbulent core is not the most sensitive indicator (temperature decay would be better), but it appears that the theory is in good agreement with ballistic-range experiments.

In this work, a number of approximations have been made so that the final results would be in a closed form, in order that the different trends for a great variety of cases could be appreciated without the need for detailed numerical calculations. On the basis of such a study, the following conclusions can be drawn:

1. All bodies produce rates of growth for the turbulent core which are higher for higher Mach numbers and hotter viscous cores. The effects of both Mach number and enthalpies prevailing at the neck

are cancelled out a few hundred diameters downstream, where the core grows with the $1/3$ power of distance multiplied by the drag coefficient and the cross section.

2. Blunted cones produce growths with more irregularities because this geometry creates overexpansions and recompressions.

3. The level of enthalpies at the neck for all bodies flying at the same altitude and Mach number is of the same order of magnitude (smaller for slender bodies after allowance is made for boundary-layer effects), but the decay of the enthalpy along the axis of the wake is faster for a cone than for a blunted body, even when both cone and blunted body may have the same total drag coefficient.

Appendix A

CALCULATION OF THE VELOCITY PREVAILING AT THE POINT ON THE
AXIS WHERE THE PRESSURE IS ALMOST AMBIENT IN
THE INVISCID WAKE OF A BLUNT BODY

In Ref. 1 it was shown that the value of the enthalpy on the axis of the wake of a blunt body and at the distance x_o where the pressure is ambient is given as

$$\frac{h_{x_o}(0)}{h_\infty} = \left(\frac{\gamma - 1}{2}\right) \left[\frac{\gamma + 1}{2\gamma}\right]^{\left(1 - \frac{1}{\gamma_L}\right)} (M^2)^{1/\gamma_L} \quad (A-1)$$

It was also shown that, independent of Mach number, $\gamma_L \approx 1.2$. It is easy to see that the quantity in brackets in Eq. (A-1) is very close to one. Hence

$$\frac{h_{x_o}(0)}{h_\infty} \approx \left(\frac{\gamma - 1}{2}\right) M^{2/\gamma_L} \quad (A-2)$$

Assuming conservation of the stagnation enthalpy, we can show that⁽¹⁾

$$f^2 \approx 1 - \frac{2}{(\gamma - 1)M^2} \left[\frac{h_{x_o}(0)}{h_\infty} - 1 \right] \quad (A-3)$$

Comparing the last two equations, we find

$$f^2 \approx 1 - \frac{1}{M \left(2 - \frac{2}{\gamma_L}\right)} \approx 1 - \frac{1}{3\sqrt{M}}$$

or

$$f \approx \sqrt{1 - \frac{1}{M^{1/3}}} \quad (A-4)$$

This relation shows that f is highly insensitive to variations in Mach number. Some values are computed in the following table:

<u>M</u>	<u>f</u>
10	0.73
15	0.77
20	0.80
25	0.81
30	0.82
35	0.83

Appendix B

INFLUENCE OF THE LAMINAR COOLING AT THE FRONT
OF THE TURBULENT WAKE

From Ref. 1 it is found that

$$\frac{h(o, X)}{h(o, o)} = \frac{1}{\left(1 + \frac{4\bar{\mu}}{\mu_{\infty}} \frac{X}{fPr\beta_o}\right)} e^{-\left(\frac{R^2}{1 + \frac{4\bar{\mu}}{\mu_{\infty}} \frac{X}{fPr\beta_o}}\right)} \quad (B-1)$$

where

$$X \equiv \frac{x/r_o}{Re} \quad \text{with} \quad Re = \frac{\rho_{\infty} U_{\infty} r_o}{\mu_{\infty}} \quad (B-2)$$

Let us choose

$$\bar{\mu}/\mu_{\infty} \sim 2, \quad f \simeq 0.8, \quad Pr = 0.7, \quad \beta_o \simeq C_D$$

Then the above becomes

$$\frac{h(o, \bar{X})}{h(o, o)} = \frac{1}{\left(1 + \frac{29\bar{X}}{C_D Re}\right)} e^{-\left(\frac{R^2}{1 + \frac{29\bar{X}}{C_D Re}}\right)} \quad (B-3)$$

Using the approximation $e^{-x^2} \simeq (1 + x^2)^{-1}$, which is compatible with Eq. (10) and the findings of Ref. 1,

$$\frac{h(o, \bar{x})}{h(o, o)} \approx \frac{1}{\left(1 + \frac{29\bar{x}}{C_D Re}\right) \left(1 + \frac{R^2}{1 + \frac{29\bar{x}}{C_D Re}}\right)} = \frac{1}{1 + R^2 + \frac{29\bar{x}}{Re C_D}} \quad (B-4)$$

The last term in the denominator can be neglected if

$$\frac{29}{Re} \frac{\bar{x}}{C_D} \ll R^2 \quad (B-5)$$

Now at large \bar{x} we have $\bar{x} \approx 2R^3$ (see Fig. 3); hence the above yields

$$\frac{29}{Re} \frac{\bar{x}}{C_D} \ll \left(\frac{\bar{x}}{2}\right)^{2/3}$$

or

$$\bar{x} \ll \frac{1}{4} \left(\frac{Re C_D}{29}\right)^3 \quad (B-6)$$

From the data of Ref. 8 the minimum Reynolds number of all experiments reported is approximately equal to 10^4 . Setting $C_D = 1.0$ we find

$$\bar{x} \ll \frac{1}{4} \left(\frac{10^4}{29}\right)^3 \approx 8.5 \times 10^6 \quad (B-7)$$

This is indeed a very high number.

Appendix C

EVALUATION OF THE FUNCTIONS A AND C_{Df} IN
TERMS OF THE HOWARTH VARIABLE R

The total drag at any given distance downstream \bar{x} , associated with the turbulent core only, is*

$$(\text{Drag})_f = 2\pi \int_0^{r_f} \rho u(u - u_f) r dr \quad (\text{C-1})$$

Through Eqs. (16), (19), and (20), the above becomes

$$(\text{Drag})_f = \frac{\pi h_\infty A(R) r_o^2 (R_{Tf})^2 \rho_f f}{2 \left(\frac{1+f}{2} \right)} \quad (\text{C-2})$$

We define a local drag coefficient C_{Df} as

$$C_{Df} = \frac{(\text{Drag})_f}{\frac{\pi r_o^2}{2} \rho_\infty U_\infty^2} \quad (\text{C-3})$$

Equation (C-2), after solving for A(R) and using Eq. (C-3), becomes

$$A(R) = \frac{C_{Df} \rho_\infty U_\infty^2}{h_\infty (R_{Tf})^2 \rho_f} \left(\frac{1+f}{2f} \right)$$

Since A(R) will only be used in the neighborhood of the axis, we have from Eq. (25)

* Assuming uniform pressure everywhere and zero velocity component in the radial direction.

$$A(R) = \frac{C_{Df} (\gamma - 1) M^2}{R_f^2} \left(\frac{1+f}{2f} \right) \quad (C-4)$$

For simplicity we assume from now on that $(1+f)/2f \approx 1.0$.

Let us assume, for the purposes of this Appendix only, that the enthalpy distribution, which includes an equivalent drag coefficient ($C_{D_{fi}}$) within the distance R_{fi} , is given by the relation

$$\frac{h(R)}{h(R=0)} = e^{-R^2/\beta}$$

We set

$$\frac{C_{Df}}{C_D} = \frac{1}{\beta} \int_0^{R_f^2} e^{-R^2/\beta} dR^2 \quad (C-5)$$

It is obvious that as $R_f \rightarrow \infty$, $C_{Df} \rightarrow C_D$ as it should. Integration yields

$$\frac{C_{Df}}{C_D} = 1 - e^{-R_f^2/\beta}$$

For small R_f we have*

$$\frac{C_{Df}}{C_D} \approx 1 - \frac{1}{1 + \frac{R_f^2}{\beta}} = \frac{R_f^2}{\beta + R_f^2}$$

* Note that the approximation $e^{-x^2} \approx 1/(1+x^2)$ is good for almost all values of x between zero and infinity, whereas $e^{-x^2} \approx 1 - x^2$ obviously is limited to values of x that are very small compared to one.

Now when $R_f = R_{fi}$, $C_{Df} = C_{Dfi}$; hence

$$\frac{C_{Df}}{C_D} = \frac{R_f^2}{\left(\frac{C_D}{C_{Dfi}} - 1\right) R_{fi}^2 + R_f^2} \quad (C-6)$$

For blunt bodies for which $C_D \gg C_{Dfi}$, the above simplifies to

$$\frac{C_{Df}}{C_D} = \frac{\frac{R_f^2}{C_D}}{\frac{R_{fi}^2}{C_{Dfi}} + \frac{R_f^2}{C_D}} \quad (C-7)$$

Appendix D

CALCULATION OF \bar{r} IN TERMS OF THE HOWARTH VARIABLE R
FOR BLUNT BODIES

The Howarth variable R is defined as

$$\rho_{\infty} R dR = \rho \bar{r} d\bar{r}$$

Assuming an ideal gas, the above is written as

$$\frac{p_{\infty}}{p} \frac{h}{h_{\infty}} dR^2 = d\bar{r}^2$$

Through Eq. (10), this reduces to

$$d\bar{r}^2 = \frac{p_{\infty}}{p} \left(1 + \frac{H}{1 + \frac{R^2}{C_D}} \right) dR^2$$

If we assume the pressure p to be constant for all R, the above integrates to

$$\bar{r}^2 = \frac{p_{\infty}}{p} \left[R^2 + C_D H \ln \left(1 + \frac{R^2}{C_D} \right) \right]$$

Appendix E

STUDY OF THE FUNCTION $\bar{r}_f(\bar{x})$ FOR DIFFERENT MACH NUMBERS AND
DIFFERENT ENTHALPIES PREVAILING AT THE
CENTER OF THE NECK OF A BLUNT BODY

Figures E-1 through E-6 show the function $\bar{r}_f(\bar{x})$ for Mach numbers 5, 7, 10, 13, 19, and 25. For each Mach number, the value of the parameter $R_{fi}^2/C_{D_{fi}}$, which depends only on the percentage λ of the stagnation enthalpy prevailing at the center of the neck according to Eq. (35), has been set equal to 3, 4, 6, 8, 10, and 12.

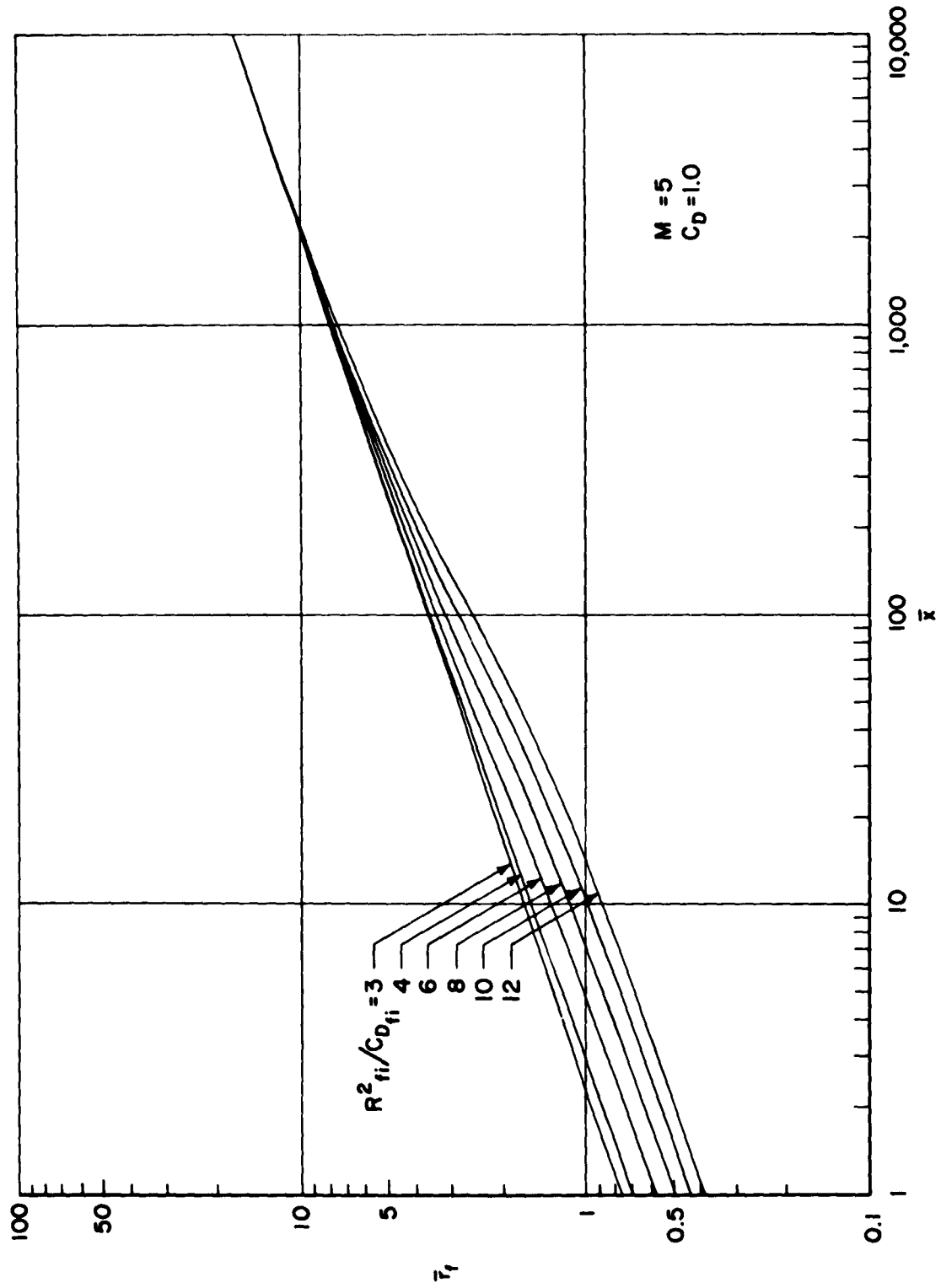


Fig.E-1—The growth of the turbulent core assuming constant pressure for $C_D=1.0$, $M=5$, and several $R^2_{ti}/C_{D_{fi}}$ values

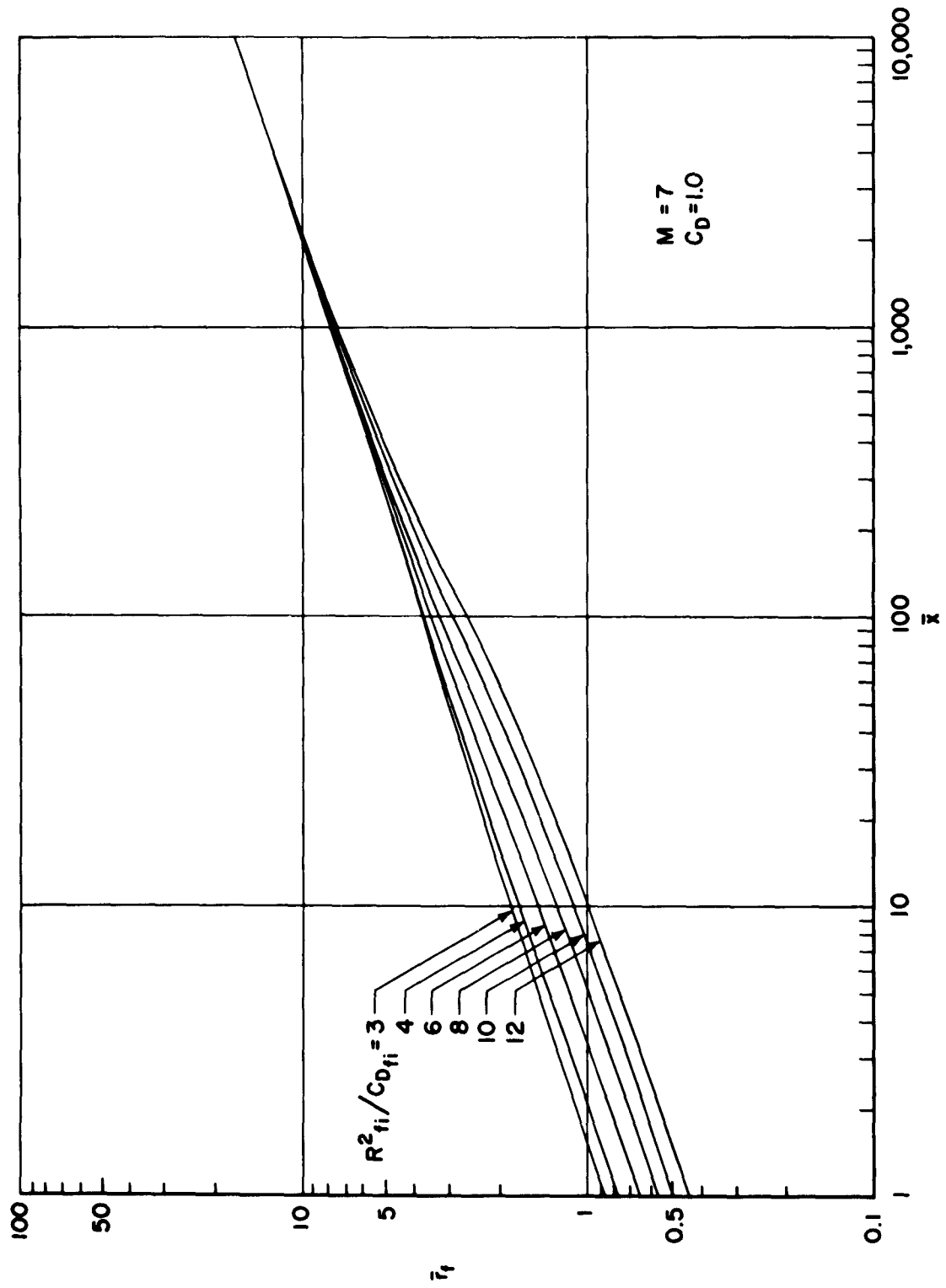
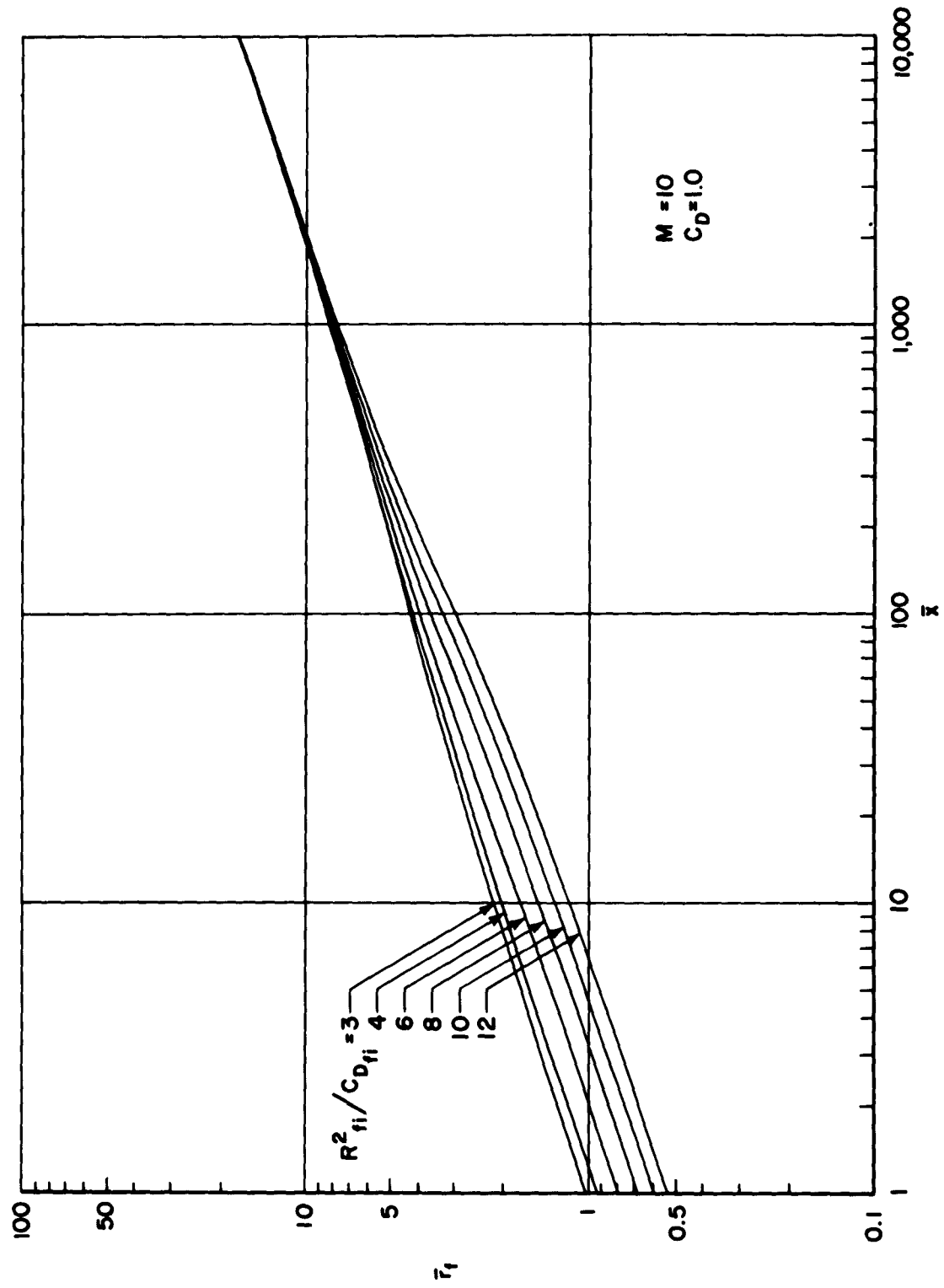


Fig.E-2—The growth of the turbulent core assuming constant pressure
for $C_D = 1.0$, $M = 7$, and several $R^2_{fi}/C_{D_{fi}}$ values



**Fig.E-3—The growth of the turbulent core assuming constant pressure
for $C_D=1.0$, $M=10$, and several $R^2_{fi}/C_{D_{fi}}$ values**

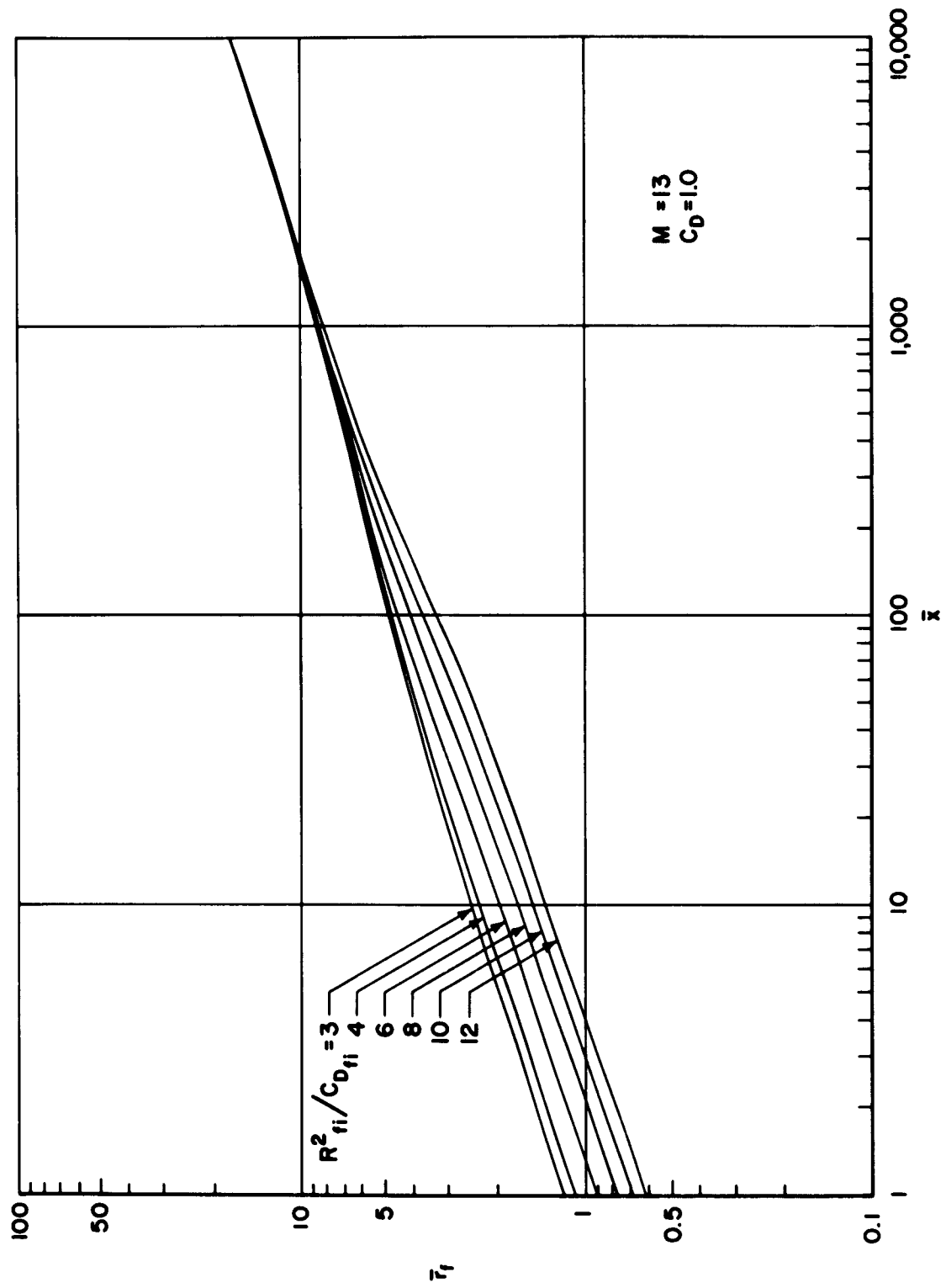


Fig.E-4—The growth of the turbulent core assuming constant pressure
for $C_D=1.0$, $M=13$, and several $R_{fi}^2 / C_{D_{fi}}$ values

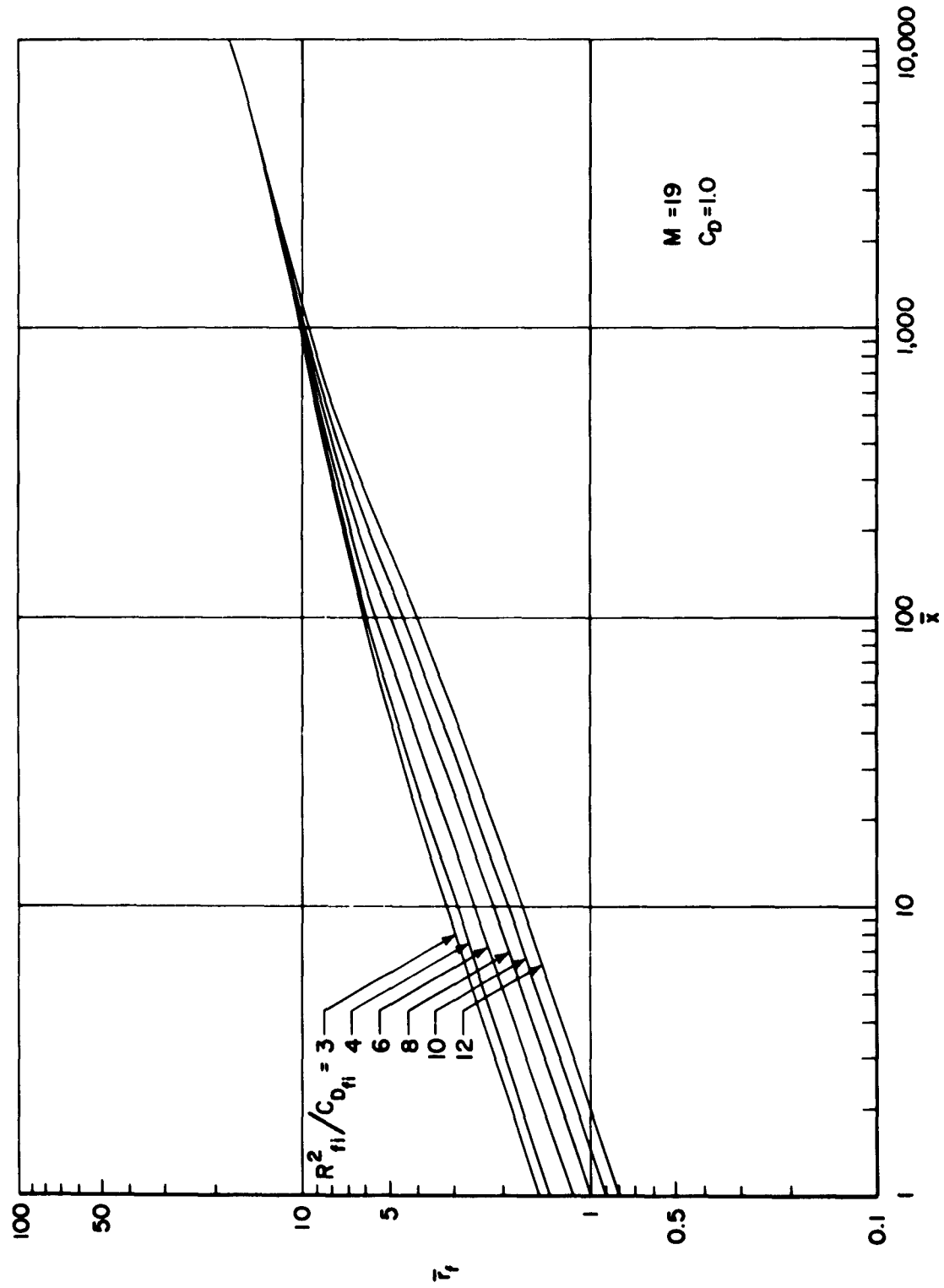


Fig.E-5—The growth of the turbulent core assuming constant pressure for $C_D=1.0$, $M=19$, and several $R_{fi}^2 / C_{D_{fi}}$ values

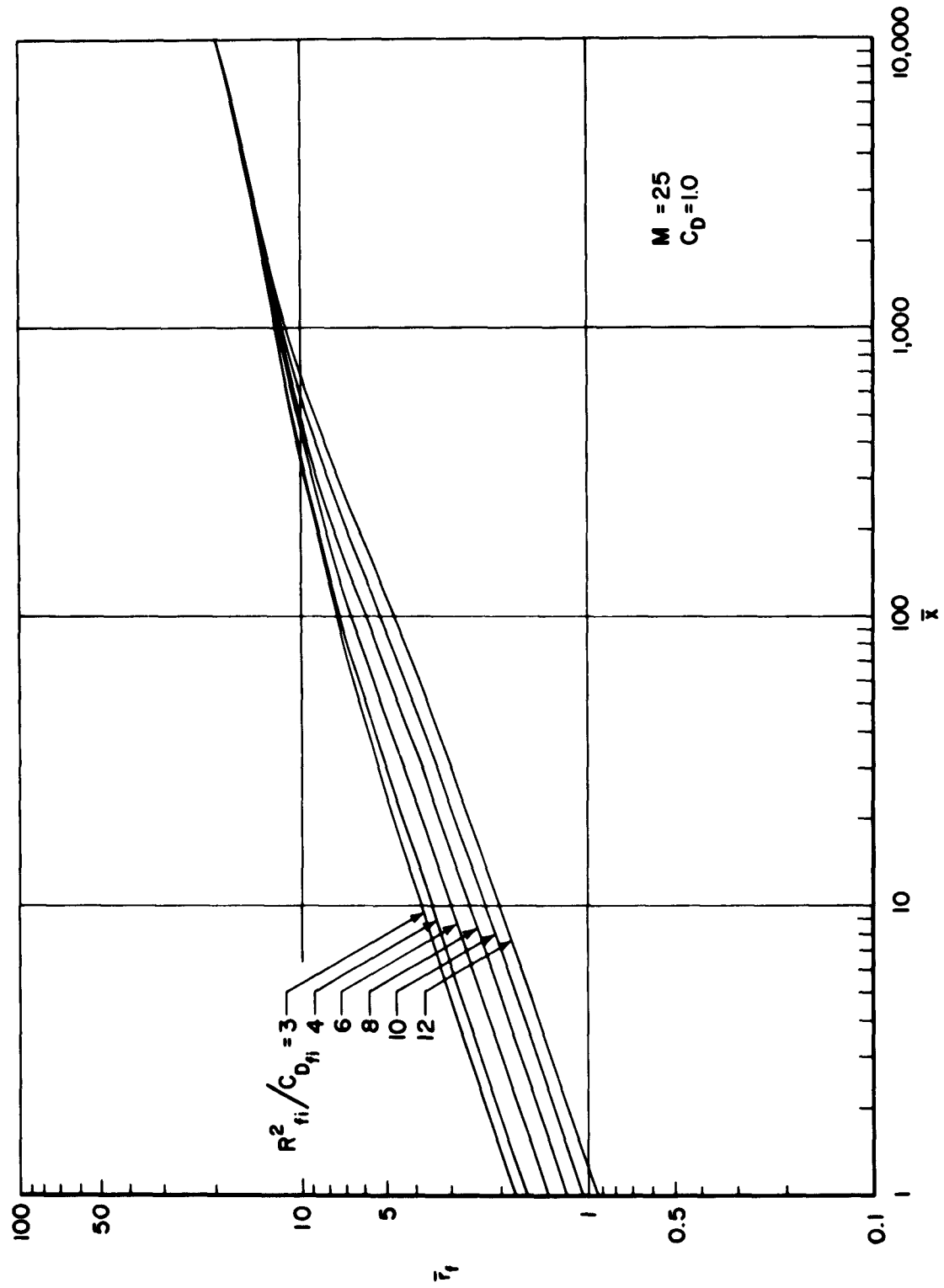


Fig.E-6—The growth of the turbulent core assuming constant pressure
for $C_D=1.0$, $M=25$, and several $R^2_{fi}/C_{D_{fi}}$ values

Appendix F

APPROXIMATION OF EQ. (39) WITH EQ. (44)

We need only to make

$$M^2 \sin^2 \beta \gg \frac{2}{\gamma - 1} \quad (F-1)$$

because we satisfy simultaneously the condition

$$M^2 \sin^2 \beta \gg \frac{\gamma - 1}{2\gamma} \quad (F-2)$$

The above statement follows from the inequality

$$\frac{2}{\gamma - 1} > \frac{\gamma - 1}{2\gamma} \quad (F-3)$$

which holds if

$$3 - \sqrt{8} < \gamma < 3 + \sqrt{8} \quad (F-4)$$

The above is always true.

Romig in Ref. 11 has found for conical flows allowing for dissociation the approximation

$$\tilde{M} \sin \beta \approx 0.39 + 1.03 \tilde{M} \sin \alpha \quad (F-5)$$

In the above, \tilde{M} is a reference Mach number defined by the relation

$$\tilde{M} = M \sqrt{\frac{T_\infty}{T_R}} \quad (F-6)$$

with $T_R = 491.7^\circ\text{K}$, and α the angle between the cone axis and the cone surface.

Making $T_{\infty} = T_R$ and using Eq. (F-5) in (F-1) we find after some algebra that inequality (F-1) is equivalent to

$$M \sin \alpha >> \frac{1.37}{\sqrt{\gamma - 1}} - 0.38 \quad (\text{F-7})$$

for $\gamma = 1.4$ the above becomes

$$M \sin \alpha >> 1.80 \quad (\text{F-8})$$

As an example, for a 20-deg cone $M >> 5.25$, and for a 10-deg cone $M >> 10.4$.

REFERENCES

1. Lykoudis, P. S., Theory of Ionized Trails for Bodies at Hypersonic Speeds, The RAND Corporation, RM-2682-1-PR, Revised October 5, 1961. A summary of this work has appeared as "Ionization Trails," in the 1961 Heat Transfer and Fluid Mechanics Institute, pp. 176-192.
2. Feldman, S., "Trails of Axi-Symmetric Hypersonic Blunt Bodies Flying Through the Atmosphere," J. Aerospace Sci., Vol. 28, No. 6, June 1961, pp. 433-448, 470.
3. Lees, L., and L. Hromas, Turbulent Diffusion in the Wake of a Blunt-Nosed Body at Hypersonic Speeds, Space Technology Laboratories, Inc., Aerodynamics Department Report No. 50, July 1961.
4. Demetriades, A., "Some Hot-Wire Anemometer Measurements in a Hypersonic Wake," Proceedings of the 1961 Heat Transfer and Fluid Mechanics Institute, Stanford University Press.
5. Ting, L., and P. A. Libby, "Remarks on the Eddy Viscosity in Compressible Mixing Flows," J. Aero. Sci., Vol. 27, October 1960, pp. 797-798.
6. Townsend, A. A., The Structure of Turbulent Shear Flow, Cambridge University Press, London, 1956.
7. Chapman, D. R., D. M. Kuehn, and H. K. Larson, Investigation of Separated Flows in Supersonic and Subsonic Streams with Emphasis on the Effect of Transition, NACA Report No. 1356, 1958 (Supersedes NACA TN 3869).
8. Slattery, R. E., and W. G. Clay, Width of the Turbulent Trail Behind a Hypervelocity Sphere, Massachusetts Institute of Technology, Lincoln Laboratory, Report No. 35. G-004, June 1961; also in Phys. Fluids, Vol. 4, 1961, pp. 1199-1201.
9. Seiff, A., and E. E. Whiting, A Correlation Study of the Bow-Wave Profiles of Blunt Bodies, NASA TN-D-1148, February 1962.
10. Slattery, R. E., and W. G. Clay, Turbulence Experiment Reentry Physics and Project PRESS Program, Semiannual Technical Summary Report to the Advanced Research Projects Agency, December 31, 1961, pp. III-9 to III-25.
11. Romig, M. F., "Applications of the Hypersonic Similarity Rule to Conical Flow of Dissociated Air," J. Aero/Space Eng., Vol. 18, March 1959, pp. 56-59, 75.
12. Hromas, L., and L. Lees, Effect of Nose Bluntness on the Turbulent Hypersonic Wake, Space Technology Laboratories, Inc., STL Report No. 6130-6259-KU-000, October 1962.